



KTH Engineering Sciences

# **A Wave Expansion Method for Aeroacoustic Propagation**

**Johan Hammar**



Licentiate Thesis  
Stockholm, Sweden  
2016

TRITA-AVE 2016:86  
ISSN 1651-7660  
ISBN 978-91-7729-215-9

---

<b>Postal address:</b>	<b>Visiting address:</b>	<b>Contact:</b>
KTH, AVE	Teknikringen 8	jhammar@kth.se
Centre for ECO <sup>2</sup> Vehicle Design	114 28 Stockholm	
SE-100 44 Stockholm		
Sweden		

---

Academic thesis with permission by KTH Royal Institute of Technology, Stockholm, to be submitted for public examination for the degree of Licentiate in Vehicle and Maritime Engineering on 15 December 2016 at 10.30 in room B1, Brinellvägen 23, KTH Royal Institute of Technology, Stockholm, Sweden.

© Johan Hammar, 2016

# Abstract

Although it is possible to directly solve an entire flow-acoustics problem in one computation, this approach remains prohibitively large in terms of the computational resource required for most practical applications. Aeroacoustic problems are therefore usually split into two parts; one consisting of the source computation and one of the source propagation. Although both these parts entail great challenges on the computational method, in terms of accuracy and efficiency, it is still better than the direct solution alternative. The source usually consists of highly turbulent flows, which for most cases will need to be, at least partly, resolved. Then, acoustic waves generated by these sources often have to be propagated for long distances compared to the wavelength and might be subjected to scattering by solid objects or convective effects by the flow. Numerical methods used solve these problems therefore have to possess low dispersion and dissipation error qualities for the solution to be accurate and resource efficient.

The wave expansion method (WEM) is an efficient discretization technique, which is used for wave propagation problems. The method uses fundamental solutions to the wave operator in the discretization procedure and will thus produce accurate results at two to three points per wavelength. This thesis presents a method that uses the WEM in an aeroacoustic context. Addressing the propagation of acoustic waves and transfer of sources from flow to acoustic simulations. The proposed computational procedure is applied to a co-rotating vortex pair and a cylinder in cross-flow. Overall, the computed results agree well with analytical solutions.

Although the WEM is efficient in terms of the spatial discretization, the procedure requires that a Moore-Penrose pseudo-inverse is evaluated at each unique node-neighbour stencil in the grid. This evaluation significantly slows the procedure and might even be more time consuming than the system matrix inversion. In this thesis, a method with a regular grid is explored to speed-up this process. Furthermore, a procedure for introducing irregular regions, while preserving the speed-up in the regular parts, is also presented.

**Keywords:** Sound propagation, Sound generation, Aeroacoustics, Aerodynamics, Computational fluid dynamics, Computational aeroacoustics, Numerical methods, Lighthill, Curle, Ffowcs Williams and Hawkings, Frequency-domain propagation, Wave expansion method.

# Sammanfattning

Även om det är möjligt att lösa både det turbulenta flödet och den akustiska utbredningen i en beräkning, så kallad "direkt simulering", så är detta fortfarande utom räckhåll för dom flesta praktiska tillämpningarna. Numeriska lösningar till aeroakustiska problem delas därför vanligen upp i två delar, en där den aeroakustiska källan beräknas, och en som hanterar ljudutbredningen från källan. Båda dessa beräkningar ställer stora krav på noggrannhet och effektivitet i beräkningsmetoden som används. Källan består ofta av starkt turbulenta flöden vilka, åtminstone delvis, måste lösas upp av den numeriska metoden. De akustiska ljudvågorna som genereras av källan transporteras sedan ofta över långa avstånd i relation till våglängden. Ljudvågorna kan då också påverkas av reflektioner mot solida väggar eller av strömningen i sig. Numeriska metoder som används för att lösa dessa problem behöver därför ha egenskaper så som små dissipation- och disperssionsfel.

Vågexpansionsmetoden (WEM) är en effektiv diskretiseringsteknik som används för att lösa vågutbredningsproblem. Metoden använder fundamentala lösningar till vågoperatoren i diskretiseringsprocessen. Det möjliggör noggranna lösningar redan vid två till tre punkter per våglängd. Den här avhandlingen beskriver hur WEM kan användas i ett aeroakustiskt sammanhang, och behandlar därför både den akustiska utbredningen, men även överföringen av källor från strömningstill akustikberäkningar. Den föreslagna beräkningsmetodiken appliceras på två olika testfall, ett som beskrivs av två motroterande virvlar och ett med en cylinder i flöde. Resultaten från båda fallen visar god överensstämmelse med analytiska referenslösningar.

Även om WEM är en effektiv diskretiseringsmetod vad gäller punkter per våglängd, så kräver metoden att en Moore-Penrose pseudoinvers utvärderas i varje unik nodstencil i beräkningsnätet. Den här utvärderingen är långsam och kan till och med ta längre tid än inverteringen av systemmatrisen. I den här avhandlingen undersöks en metod baserad på ett reguljärt beräkningsnät för att snabba upp processen. Vidare utforskas även en procedur för att inkludera icke-reguljära regioner, vilken bibehåller möjligheten att snabba upp den totala processen.

**Nyckelord:** Ljudutbredning, ljudalstring, aeroakustik, aerodynamik, computational fluid dynamics, numeriska metoder, Lighthill, Curle, Ffowcs Williams and Hawkings, Wave expansion method.

# Acknowledgements

Firstly, I would like to express my sincerest gratitude to my supervisors Gunnilla Efraimsson and Ciarán O'Reilly for your guidance and support. You have always been available and encouraged me through this work. I highly value all the knowledge you have shared in our discussions and the positive attitude which you spread to your surrounding.

I would also like to thank all my colleagues at Creo Dynamics and KTH for all the interesting discussions and for providing an enjoyable atmosphere. I would especially like to thank Gustav Kristiansson and Urban Emborg who believed in this project from the start and have always encouraged the work within research and innovation at Creo Dynamics.

Thank you to my mother and father for all your encouragement. And also for the help and support, getting the day to day life to work smoothly.

Finally, I would like to thank my family and my wonderful wife Christin who has supported me throughout this project.

This work has been funded through the Swedish Vinnova program, Nationellt Flygtekniskt Forsknings Program NFFP6 and is part of the Methods for Improved Accuracy of Unsteady aerodynamics MIAU project. Partners of this project are Creo Dynamics, Saab, FOI, KTH, Chalmers and Linköping University. I gratefully acknowledge the funding of the project and would also like to express my gratitude to all the partners of the project.

I would also like to acknowledge the Centre for ECO<sup>2</sup> Vehicle Design at KTH of which this work has been a part. The centre is a great place to be a PhD student.



# Dissertation

This thesis consists of two parts. The first part gives an overview of the research area and work performed. The second part contains the appended research papers (A–B).

## Paper A

J. Hammar, C. J. O’Reilly and G. Efrainsson *Simulation of Aerodynamically Generated Noise Propagation Using the Wave Expansion Method*. AIAA/CEAS Aeroacoustic conference, Lyon, 2016

J. Hammar developed the method, implemented it and wrote the paper. C. J. O’Reilly and G. Efrainsson supervised the work and discussed ideas and reviewed the paper.

## Paper B

J. Hammar, C. J. O’Reilly and G. Efrainsson *Speed up of assembly for wave expansion method using a uniform background mesh*.

J. Hammar developed the method, implemented it and wrote the paper. C. J. O’Reilly and G. Efrainsson supervised the work and discussed ideas and reviewed the paper.

## Publications not included in this thesis

J. Hammar, C. J. O’Reilly and G. Efrainsson. *Simulation of Aerodynamically Generated Sound Using Hybrid Aeroacoustic Method*. Euronoise, 10th European Congress and Exposition on Noise Control Engineering, Maastricht, Netherlands, 2015.

# Contents

<b>I OVERVIEW</b>	<b>1</b>
<b>1 Introduction</b>	<b>3</b>
1.1 Relevance to Industry and Society . . . . .	3
1.2 Aeroacoustic approaches . . . . .	4
1.2.1 Direct . . . . .	4
1.2.2 Hybrid . . . . .	5
1.3 Simulation methods . . . . .	5
1.3.1 Flow . . . . .	6
1.3.2 Analytical propagation . . . . .	6
1.3.3 Numerical propagation . . . . .	7
1.4 Proposed method . . . . .	8
1.5 Scope of work . . . . .	9
1.6 Contributions . . . . .	9
<b>2 Aeroacoustic analogies</b>	<b>11</b>
2.1 Lighthill . . . . .	11
2.2 Green's function solution . . . . .	12
2.3 Curle's equation . . . . .	15
2.4 Ffowcs Williams and Hawkings . . . . .	16
2.5 Vortex Sound . . . . .	18
2.6 Conclusions . . . . .	19
<b>3 The Wave Expansion Method</b>	<b>21</b>
3.1 Discretization . . . . .	22
3.2 Planewave formulations . . . . .	23
3.3 Boundary conditions . . . . .	25
3.3.1 Dirichlet . . . . .	25
3.3.2 Neumann . . . . .	25
3.3.3 Radiation . . . . .	25
<b>4 Introduction of sources</b>	<b>27</b>

4.1	Point sources . . . . .	27
4.2	Distributed CFD sources . . . . .	29
4.3	Co-rotating vortex pair . . . . .	30
4.3.1	Analytical solution . . . . .	31
4.3.2	Numerical solution . . . . .	32
4.4	Cylinder in cross-flow . . . . .	34
4.4.1	Flow solution . . . . .	35
4.4.2	Acoustic solution . . . . .	36
4.5	Conclusions . . . . .	40
<b>5</b>	<b>Fast matrix assembly technique</b>	<b>43</b>
5.1	Process for background matrix . . . . .	43
5.1.1	Plane wave in a pipe . . . . .	44
5.2	Process with irregular region . . . . .	46
5.2.1	Local remeshing . . . . .	47
5.3	Conclusions . . . . .	49
<b>6</b>	<b>Summary and Outlook</b>	<b>51</b>
6.1	Conclusions . . . . .	51
6.2	Reflections and limitations . . . . .	51
6.3	Future work . . . . .	53
	<b>Bibliography</b>	<b>55</b>
<b>II</b>	<b>APPENDED PAPERS</b>	<b>59</b>



**Part I**

**OVERVIEW**



# 1

## Introduction

In this chapter the proposed method and scope of work is stated together with a discussion of the background to flow noise and its simulation. The background includes importance in industrial application and the simulation techniques that are relevant within the subject. Finally a simulation method is proposed and the contributions to this method are described.

### 1.1 Relevance to Industry and Society

Aeroacoustic simulations are an important part in the development of quiet products and transportation. More and more focus is directed towards avoiding or reducing aeroacoustic noise in the development of transportation. Driving this development are the customer's requirements on quieter products, and legislation requirements aiming to lessen the environmental impact of the noise from traffic, trains and aircraft. As an example, reduction of external noise is one of the priority areas in the Strategic Research Agenda of ACARE Vision 2020<sup>1</sup>. For external noise, the goal is to reduce the perceived external noise to half of the levels of 2001, which is when the report was published. Due to changes in recent years' additional goals have also been presented towards the year of 2050. This new vision, Flightpath 2050<sup>2</sup> was released in 2011 and further highlights the research needs of the years to come.

The possibility to use aeroacoustic simulations in the design process is also of high importance to the industry. As they enable designs to be analysed in an early design phase, reducing the risk of late changes which are usually much costlier.

Simulations can also give a detailed insight to the physical problem and therefore present new solutions.

Due to these demands, research within aeroacoustics has grown considerably during recent decades<sup>3</sup>. Computational aeroacoustics is now part of the product development process at many aircraft and vehicle manufacturers. The most frequent areas of research within aeroacoustics are still related to the aircraft industry, where noise legislation close to airports is driving the research for the design of quiet aircraft. Furthermore, high speed trains and the vehicle industry are also subjected to noise legislation, which increases the need for better testing and simulation methods.

For small and medium size companies such as Creo Dynamics, efficient simulation methods are a key element to perform parametric studies and evaluate new innovative ideas. The aeroacoustic testing can be very expensive, especially if wind tunnels or complex lab environments are needed. Direct simulations are tempting, since they reveal much details of the physical problem. However, massive computer resources are often required to solve the flow-acoustic fields directly. Turbulence-resolving flow simulations on the other hand are becoming a natural part of the aerodynamic analysis. Linear propagation methods with sources based on these CFD simulations are therefore a very attractive alternative.

## 1.2 Aeroacoustic approaches

### 1.2.1 Direct

Aeroacoustic problems are complex by nature and the description of the source characteristics is far from trivial. The compressible flow equations which govern the fluid motion also includes the acoustic perturbations. To solve these equations for the whole region of interest, retaining both the flow and acoustic fields, is generally referred to as direct simulation in aeroacoustics<sup>4</sup>. Although the possibility to perform large scale computations has expanded the region in which these simulations are possible, they are still prohibitively expensive for most cases. Many challenges exists for such computations. For example, the difference in scales of the pressure fluctuations in hydrodynamic near field and the pressure in the acoustic far field. This is usually many orders of magnitude, which makes it very challenging for a numerical method. Another challenge is that the acoustic waves must usually be propagated for long distances compared to the extent of the source region. A high spatial resolution will therefore be needed in a very large domain. A further discussion regarding the requirements for direct simulations within aeroacoustics is given in Tam<sup>5</sup>.

### 1.2.2 Hybrid

Due to the challenges associated with direct simulations, the source computation and propagation are usually decoupled. This is referred to as a hybrid treatment and is convenient, since it allows the flow and acoustic propagation to be solved individually. Appropriate methods and numerical schemes can then be used for each of these parts separately, avoiding some of the challenges faced with direct simulation.

#### Acoustic analogy

The most common way to form a hybrid method is to use an acoustic analogy. The rearrangement of the flow equations in the form of an analogy was first proposed by Lighthill<sup>6,7</sup> and has since its introduction been the starting point for a major part of flow induced noise computations. Lighthill's analogy considers aeroacoustic sources in an unbounded flow, such as a turbulent jet. The understanding of jet noise scaling resulting from this approach was also one of the significant contributions of the work by Lighthill.

Further development by Curle<sup>8</sup> yielded an equation where the effect of solid surfaces is included in the solution. These are accounted for by sources introduced at the surfaces. Curle's solution has then also been extended to account for the effect of source motion in the analogy by Ffowcs Williams and Hawkings<sup>9</sup>, which for example allowed the inclusion of rotating blades for fans and rotors.

Vortex-based analogies have also been formulated from Lighthill's analogy by for instance Powell<sup>10</sup> and Howe<sup>11</sup>. The vortex-based analogies are derived in a similar approach as Lighthill's analogy. However, the vortex formulation highlights the role of convected vorticity as a source of sound. This formulation might give a less extended source region than the sources in Lighthill's analogy and could therefore present an advantage in numerical simulations. However, it has also been argued that this formulation is more sensitive to numerical errors in the source description, which on the other hand would present a weakness. A further discussion regarding the robustness of these sources is given by Martínez-Lera et. al.<sup>12</sup>. The vortex sound theory also presents a natural way of relating the acoustic propagation to a potential flow.

## 1.3 Simulation methods

In hybrid simulations, the non-linear flow equations will give the solution in the source region. From these sources linear propagation equations can be used to evaluate the acoustic field. A schematic illustration of methods used for aeroacoustic computations is shown in Figure 1.1, where the parts related to this work are marked in bold font.

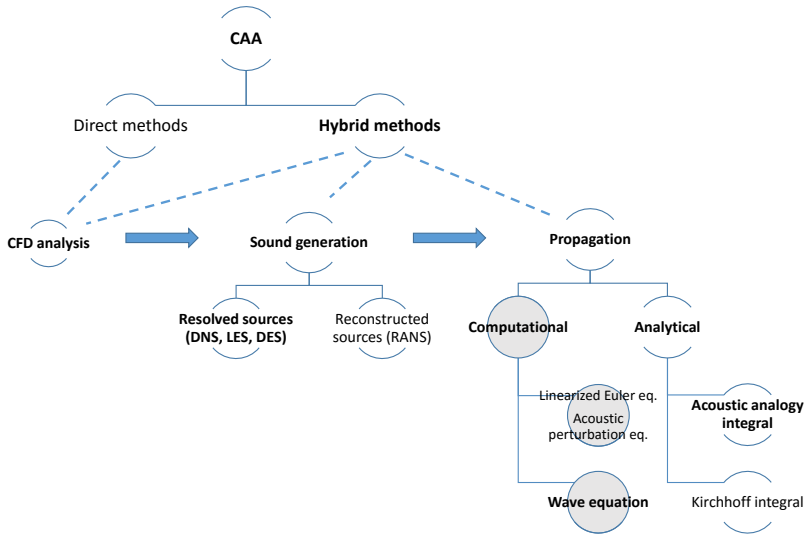


Figure 1.1. Aeroacoustic simulation methods

### 1.3.1 Flow

The computation of the source region is a very complex problem which usually results in resolving highly turbulent flows. It is usually not possible to resolve all the turbulent scales. Instead the smallest scales of isotropic turbulence are modelled using large eddy simulation (LES) methods<sup>13</sup>. The simulation and modelling of these flows is not reviewed to any greater extent in this work. Although it should be mentioned, that when simulations are used to describe the sources, the accuracy of these computations will be essential for the acoustic field to be correct.

### 1.3.2 Analytical propagation

For many cases, the most efficient application of aeroacoustic analogies is to assume that the source region is compact and that the listener is located in a quiescent flow, to which the sound waves can propagate freely. This assumption is particularly valid in very low-Mach-number flows when the source is compact (i.e. the wavelength is long with regard to the considered object) and the sound is not scattered by any solid object. For these cases the solution of the analogies can often be found using the free-field Green's function. The acoustic pressure at the listener's location can then be calculated using an integral solution of the source

propagation. A recent formulation of such a procedure is found in Nayafi-Yasdi et. al.<sup>14</sup>, solving for moving sources in a uniform moving media.

In a more general case, where the scattering by the flow or solid objects is not negligible, a tailored Green's function is needed to account for the boundaries in the acoustic propagation. Howe<sup>11</sup> describes the derivation of tailored Green's functions for a number of model problems. In cases with complex geometry, these methods become highly complicated. The use is therefore limited to generic geometries.

### 1.3.3 Numerical propagation

The aeroacoustic analogy can also be formulated as a boundary value problem (BVP), which is solved numerically. This will give more flexibility and avoid the analytical treatment in the Green's function integral formulation. Many well established methods exist for the solution of these linear propagation problems, such as the finite difference method (FDM), finite element method (FEM) and the boundary element method (BEM). All these methods have their advantages and short comings. The FDM is quite straight forward to implement. However, it requires the use of a smooth grid which can impose restrictions on the grid generation. The FEM is less sensitive to the element shape and thus more applicable to practical applications. Both the FEM and the FDM require that the full domain is discretized. This will result in a large system matrix that needs to be inverted. The BEM, on the other hand, only requires the surfaces to describe the problem, which will result in a smaller system matrix. However, this matrix will be densely populated and is therefore more difficult to solve.

The FEM has been used in numerous aeroacoustic applications. The formulations usually involves solving the variational form of Lighthill's analogy, proposed by Oberai<sup>15</sup>. Versions of this approach have also been further developed in recent years and are part of some of the leading commercial software in the field, such as LMS Virtual Lab and Actran. A challenging part of these formulations is the transfer of sources from the flow simulation to the acoustic propagation solver. The flow solver generally requires a much finer mesh in the source region, especially if the different solvers are to be used efficiently.

Since the volume is discretized in FDM and FEM, a spatially varying mean flow can be included in the acoustic computations, to account for the effect of convection. In the BEM, only homogeneous flow effects can be included. This is done by using Prandtl-Glauert transformation. In general this restricts the use of the BEM slightly more in terms of the turbulent source compactness. If the turbulent source region is spatially extended in comparison to the wavelength, the scattering by the flow might not be negligible. Khalighi<sup>16</sup> recently showed a BEM formulation related to an aeroacoustic analogy. By using the BEM to solve the acoustic propagation, scattering by objects can be included. The method will therefore also

avoid part of the compactness limitation which normally restrict the frequency range of integral methods.

The numerical methods mentioned above all suffer from dispersion-type errors. This means that many points are needed to accurately resolve the acoustic waves. In the use of second order FEM and FDM, a range of 7 to 10 points per wavelength is usually recommended. Higher-order methods (HOM) can be used to decrease this number. However, these are more challenging to implement and may also increase the size or bandwidth of the systems matrix. Examples of higher-order methods with low dispersion-error properties can be found in Tam<sup>17</sup>, Bogey and Bailly<sup>18</sup> and Efraimsson et. al.<sup>19</sup>.

## 1.4 Proposed method

The Wave Expansion Method (WEM) is a very efficient discretization method for solving acoustic propagation described by linear time-harmonic equations. It is rather easy to implement and does not suffer from dispersion-type errors. The grey areas in Figure 1.1 illustrate problems to which this type of method can be applied.

The WEM is based on the Green's function discretization that was firstly developed by Caruthers et. al.<sup>20</sup>. In that work the use of a local wave expansion stencil was proposed and developed for the solution of the Helmholtz equation. The results showed great promise in the number of grid points needed to resolve acoustic waves. Later the method was also applied to acoustic propagation through an inhomogenous flow field, showing the application to acoustic propagation in a aero-engine nacelle<sup>21:22</sup>. The utilization was mostly focused on two dimentions untill Ruiz and Rice<sup>23</sup> explored its application to three space dimensions, also introducing a free radiation boundary conditions, further highlighting the advantages of the discretization technique. A forward-advancing implementation was developed by Barrera Rolla and Rice<sup>24</sup> where backscattering was neglected to enable large-scale problems such as long-range atmospheric propagation. The method has recently been further developed by O'Reilly<sup>25:26</sup> who introduced a flow-impedance boundary condition for the application to lined ducts. Liu<sup>27</sup> also added a method to introduce a point source with the application to car interior acoustics.

In general the method has showed to be highly efficient in solving acoustic wave propagation. The method has been shown to give accurate solutions down to a spatial resolution of two points per wavelength. These properties make the WEM very suitable for aeroacoustic problems where the acoustic propagation can be solved as a linear propagation. Although the WEM is efficient, it is not nearly as well investigated as for example the FEM. There are still parts of the method that needs to be investigated further or improved. Two of these are the implementation of sources and the local pseudo-inverse that needs to be evaluated at each node

as the stiffness matrix is assembled. For the method to work in the context of an aeroacoustic analogy these gaps need to be addressed.

## 1.5 Scope of work

This work aims at using the WEM in the context of aeroacoustic analogies. To do this, aeroacoustic sources need to be introduced in the method. Firstly, simple point sources are introduced, with and without a convective mean flow. These are then extended to more complicated source regions based on analytical solutions and CFD computations. As a first stage this is solved as a free-radiation problem. However, the long term goal is to include scattering and inhomogeneous flow in the acoustic WEM solution, allowing the method to be used without the limitation of compact geometries and source regions.

## 1.6 Contributions

The main contributions of this thesis related to the development of the WEM are

- A method to introduce sources of different character such as monopole, dipole and quadrupole into the acoustic propagation simulation.
- Introduction of sources in an acoustic propagation with convection effects from a mean flow.
- Solution of acoustic propagation with sources from CFD based on an aeroacoustic analogy.
- A method to speed-up the assembly process by using regions of regular grid.



# 2

## Aeroacoustic analogies

The aeroacoustic analogy is a concept that has its origin in the 50s when there was a need to bring further light to the source of jet noise from aircraft. Aeroacoustic analogies started with the reformulation of the flow equations in the form of an inhomogeneous wave equation by Lighthill. From this, the famous  $U^8 - law$  gave much insight, describing the scaling of relevant parameters for jet noise. Since then, Lighthill's analogy has been further developed by numerous researchers who have contributed by expanding or reformulating it to be applicable to other cases and conditions. The formulations of some of the most important aeroacoustic analogies are described in this chapter, more detailed descriptions are found in Howe<sup>11;28</sup> and Hirschberg and Rienstra<sup>29</sup>. A short description of the use of Green's functions to solve acoustic equations is also given.

### 2.1 Lighthill

The derivation of Lighthill's analogy<sup>7</sup> starts at the equations for fluid flow known as the Navier-Stokes equations, conservation of mass and momentum. These are given by

$$\frac{\partial \rho}{\partial t} + \frac{\partial \rho u_i}{\partial x_i} = m \quad (2.1)$$

$$\frac{\partial \rho u_i}{\partial t} + \frac{\partial \rho u_i u_j}{\partial x_j} = -\frac{\partial p}{\partial x_i} + \frac{\partial \tau_{ij}}{\partial x_j} + f_i \quad (2.2)$$

where  $\rho$  is the density,  $t$  is the time,  $u$  is the velocity,  $p$  is the pressure,  $\tau_{ij}$  is the viscous stress tensor,  $m$  is a mass source and  $f_i$  is a momentum source. These equations describe the motion of the fluid flow, including also the acoustic perturbations. To form a wave equation, the time derivative of Equation (2.1) is added to the spatial derivative of Equation (2.2),

$$\frac{\partial^2 \rho'}{\partial t^2} = \frac{\partial m}{\partial t} - \frac{\partial f_i}{\partial x_i} + \frac{\partial^2}{\partial x_i \partial x_j} (\rho u_i u_j + p' \delta_{ij} - \tau_{ij}), \quad (2.3)$$

where the fluctuation are described by  $\rho = \rho' + \rho_0$  and  $p = p' + p_0$ . Primed quantities therefore denote fluctuations around a mean, which is denoted by 0. By subtracting the second spatial derivative of the pressure fluctuation on both sides and substituting  $\rho$  with  $p/c_0^2$ , assuming homentropic conditions, Equation (2.3) may be written as

$$\frac{\partial^2 \rho'}{\partial t^2} - c_0^2 \frac{\partial^2 \rho'}{\partial x_i \partial x_i} = \frac{\partial m}{\partial t} - \frac{\partial f_i}{\partial x_i} + \frac{\partial^2 T_{ij}}{\partial x_i \partial x_j} \quad (2.4)$$

where  $T_{ij}$  is the Lighthill stress tensor

$$T_{ij} = \rho u_i u_j + (p' - c_0^2 \rho') \delta_{ij} - \tau_{ij} \quad (2.5)$$

This equation has a LHS that corresponds to a wave equation and a RHS that can be considered as an aeroacoustic source. It should be noted that no restrictions are posed on the perturbations to be small. In fact, this means that Equation (2.4) is still just as difficult to solve as the flow equations. However, if a listener in a quiescent region of the field is considered, the RHS would be vanishing in this region. The remaining part will therefore consist of a wave equation. Thus it makes sense to regard the field in two regions; one where the RHS is non-zero, also referred to as a source region; and one where the RHS is zero, here the field will describe propagation of acoustic waves.

The region decomposition shown in Figure 2.2 is an important part of Lighthill's analogy and implies that the source on the RHS can be treated separately, if it is assumed to be unaffected by the acoustic propagation. This is usually used in computational aeroacoustics where the source region is computed using methods suitable for flow simulations and the acoustic propagation is then treated separately assuming that the RHS is known.

## 2.2 Green's function solution

With the use of Green's theorem, one can construct an integral equation which combines the effect of sources, propagation, boundary conditions and initial conditions. In the case that the source  $q$  is known, the convolution of the source and

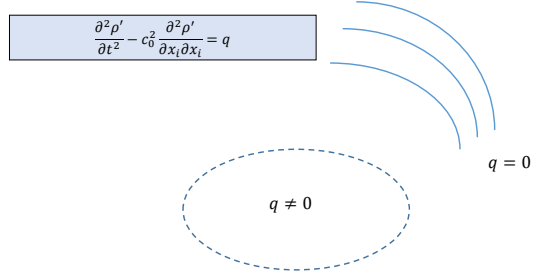


Figure 2.1. Acoustic regions.

the Green's function  $G$  will give an explicit solution to the wave equation of the form,

$$\rho'(\mathbf{x}, t) = \int_{-\infty}^t \int_V q(\mathbf{y}, \tau) G(\mathbf{x}, t | \mathbf{y}, \tau) d^3\mathbf{y} d\tau. \quad (2.6)$$

where  $\mathbf{x}$  and  $\mathbf{y}$  are the locations of the receiver and source,  $t$  is the time and  $\tau$  is the time at the source. However, if  $q$  is dependent on  $\rho'$  these are integral equations and not a explicit solution any more. The Green's function also has to satisfy boundary conditions which make it very difficult to find for a general case. The use of the Green's function is therefore usually restricted to cases of a free-field radiation or cases where simpler descriptions of the geometrical boundaries can be applied. Although this might sound very restrictive, it has still proven to be very useful in many cases and the free-field Green's function is widely used in aeroacoustics today. The free-field Green's functions in two-dimensions is defined as the impulse response,

$$\left( \frac{\partial^2}{\partial t^2} - c_0^2 \frac{\partial^2}{\partial x_i \partial x_j} \right) G_0(\mathbf{x}, t; \mathbf{y}, \tau) = \delta(\mathbf{x} - \mathbf{y}) \delta(t - \tau), \quad (2.7)$$

and is given by

$$G_0(\mathbf{x}, t; \mathbf{y}, \tau) = \frac{H(c_0(t - \tau) - |\mathbf{x} - \mathbf{y}|)}{2\pi c_0 \sqrt{c_0(t - \tau)^2 - |\mathbf{x} - \mathbf{y}|^2}} \quad (2.8)$$

where  $H$  is the Heaviside function. In frequency domain the Green's function for the Helmholtz equation

$$\left( \frac{\partial^2}{\partial x_i \partial x_i} + k^2 \right) \hat{G}_0(\mathbf{x}, \mathbf{y}, \omega) = \delta(\mathbf{x} - \mathbf{y}) \quad (2.9)$$

will be

$$\hat{G}_0(\mathbf{x}, \mathbf{y}, \omega) = \frac{-i}{4} H_0^{(2)}(k|\mathbf{x} - \mathbf{y}|) \quad (2.10)$$

here  $H_0^{(2)}$  is the Hankel function of order zero and second kind and  $k$  is the wave number. To account for the convection of a mean flow, a Prandtl-Glauert transformation can be used to transform the convected Helmholtz equation,

$$\left\{ \frac{\partial^2}{\partial x_i^2} + k^2 - 2iM_i k \frac{\partial}{\partial x_i} - M_i M_j \frac{\partial^2}{\partial x_i \partial x_j} \right\} \hat{G}_0(\mathbf{x}, \mathbf{y}, \omega) = \delta(\mathbf{x} - \mathbf{y}), \quad (2.11)$$

to the Helmholtz equation with the following free-field Green's function,

$$\hat{G}(\mathbf{x}, \mathbf{y}, \omega) = \frac{i}{4\beta} e^{i(Mk(x_1 - y_1)/\beta^2)} H_0^{(2)}\left(\frac{k}{\beta^2} r_\beta\right) \quad (2.12)$$

where  $r_\beta = \sqrt{(x_1 - y_1)^2 + \beta^2(x_2 - y_2)^2}$ ,  $\beta = \sqrt{1 - M^2}$  and  $M$  is the Mach number.

The Green's functions shown so far will work perfectly well to give a solution to a distribution of monopole sources. Which would typically correspond to a fluctuating mass injection. In the aeroacoustic analogies, the sources are also of multi-pole character, such as dipole and quadropole. Multi-pole sources can either be constructed using multiple monopole sources, or the derivatives of these sources can be transferred to the Green's function. If we consider the quadropole source term by Lighthill,  $\partial^2 T_{ij}/\partial x_i \partial x_j$ , and neglect the other sources. The frequency domain solution based on the Green's function will be,

$$\hat{p}(\mathbf{x}, \omega) = \int_V \frac{\partial^2 T_{ij}}{\partial x_i \partial x_j} \hat{G}_0 d^3 \mathbf{y}. \quad (2.13)$$

By applying partial integration twice the derivative will be on the Green's function,

$$\hat{p}(\mathbf{x}, \omega) = \int_V T_{ij} \frac{\partial^2 \hat{G}_0}{\partial x_i \partial x_j} d^3 \mathbf{y}. \quad (2.14)$$

This is still the same solution. However, from a computational perspective it can have some important implications. The Lighthill tensor,  $T_{ij}$ , is often computed using a numerical method. If the derivative is taken on the Lighthill tensor, it will be evaluated using the numerical method, which might introduce numerical errors. If the derivative is instead transferred to the Green's function, it can be described using the analytical solution. The first and second derivative of the free-field Green's function will be of the form,

$$\frac{\partial \hat{G}_0}{\partial x_i} = \frac{ik}{4} H_1^{(2)}(k|\mathbf{x} - \mathbf{y}|) \quad (2.15)$$

and

$$\frac{\partial^2 \hat{G}_0}{\partial x_i \partial x_j} = \frac{ik^2}{4} \left( H_0^{(2)}(k|\mathbf{x} - \mathbf{y}|) - \frac{H_1^{(2)}(k|\mathbf{x} - \mathbf{y}|)}{k|\mathbf{x} - \mathbf{y}|} \right). \quad (2.16)$$

The Prandtl-Glauert transformation described previously can be used to include the effect of a mean flow in these Green's functions with derivatives.

### 2.3 Curle's equation

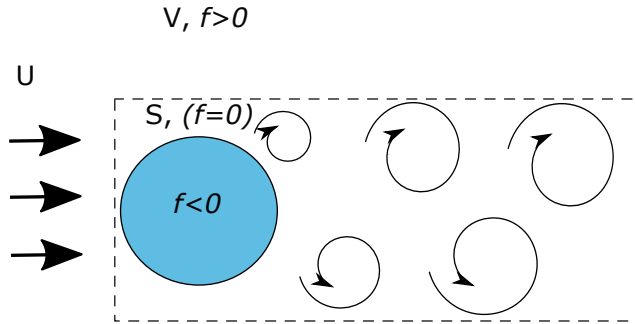


Figure 2.2. Flow domain regions used in Curle's equation.

Lighthill's theory is formulated to consider free-field turbulent flows and sound propagation to a listener in a quiescent field. However, it is common that surfaces are present in the source region. Curle derived a solution to Lighthill's analogy referred to as Curle's equation<sup>8</sup>. In this derivation a surface is defined by using a function  $f(\mathbf{x})$ ,

$$f(\mathbf{x}) = 0, \text{ where } \begin{cases} f(\mathbf{x}) > 0 & \text{for } \mathbf{x} \text{ in } V, \\ f(\mathbf{x}) < 0 & \text{for } \mathbf{x} \text{ within } S. \end{cases} \quad (2.17)$$

and the Heaviside unit function of  $f$ , which is then,

$$H(f) = \begin{cases} 1 & \text{for } \mathbf{x} \text{ in } V, \\ 0 & \text{for } \mathbf{x} \text{ within } S. \end{cases} \quad (2.18)$$

By introducing  $H \equiv H(f)$  in the momentum and continuity equation and using a similar process as in Lighthill's analogy, a differential form of Curle's equation is given by

$$\begin{aligned} \left( \frac{1}{c_0^2} \frac{\partial^2}{\partial t^2} - \nabla^2 \right) [Hc_0^2 \rho'] \\ = \frac{\partial^2 (HT_{ij})}{\partial x_i \partial x_j} - \frac{\partial}{\partial x_i} \left( (\rho u_i u_j + p'_{ij}) \frac{\partial H}{\partial x_j} \right) + \frac{\partial}{\partial t} \left( \rho u_j \frac{\partial H}{\partial x_j} \right) \end{aligned} \quad (2.19)$$

This differential equation can be formulated as an integral equation yielding Curle's equation.

$$\begin{aligned} Hc_0^2 \rho' = \frac{\partial^2}{\partial x_i \partial x_j} \int_V [T_{ij}]_{t_e} \frac{d^3 \mathbf{y}}{4\pi |\mathbf{x} - \mathbf{y}|} - \frac{\partial}{\partial x_i} \oint_S [\rho u_i u_j + p'_{ij}]_{t_e} \frac{dS_j(\mathbf{y})}{4\pi |\mathbf{x} - \mathbf{y}|} \\ + \frac{\partial}{\partial t} \oint_S [\rho u_j]_{t_e} \frac{dS_j(\mathbf{y})}{4\pi |\mathbf{x} - \mathbf{y}|}, \end{aligned} \quad (2.20)$$

where  $t_e$  denotes that the variables should be evaluated at emission time and  $p'_{ij} = p' \delta_{ij} - \tau_{ij}$ . In this formulation the surface does not have to coincide with a solid surface. The position of the surface is therefore still possible at an arbitrary location. However, if the surface is restricted to solid surfaces this expression can be significantly simplified giving the following integral formulation,

$$Hc_0^2 \rho' = \frac{\partial^2}{\partial x_i \partial x_j} \int_V [T_{ij}]_{t_e} \frac{d^3 \mathbf{y}}{4\pi |\mathbf{x} - \mathbf{y}|} - \frac{\partial}{\partial x_i} \oint_S [p'_{ij}]_{t_e} \frac{dS_j(\mathbf{y})}{4\pi |\mathbf{x} - \mathbf{y}|}, \quad (2.21)$$

In Curle's equation a surface integral will appear which includes the surface dipole sources. In bounded low-Mach number flows these are often regarded as the most significant sources. Therefore, the volume integral over the quadropole sources is often discarded, which simplifies the equations further.

## 2.4 Ffowcs Williams and Hawkings

Letting the surface from the derivation of Curle's equation include a motion, Equation (2.19) needs to be rewritten. This is useful in many aeroacoustic applications where the noise is generated by spinning or translating objects. To do this a velocity  $\mathbf{v}$  is used to describe the surface velocity. The differential equation of Ffowcs Williams and Hawkings<sup>9</sup> can then be attained in a similar way as for

Curle's equation,

$$\begin{aligned} & \left( \frac{1}{c_0^2} \frac{\partial^2}{\partial t^2} - \nabla^2 \right) [Hc_0^2 \rho'] \\ &= \frac{\partial^2 (HT_{ij})}{\partial x_i \partial x_j} - \frac{\partial}{\partial x_i} \left( (\rho u_i (u_j - v_j) + p'_{ij}) \frac{\partial H}{\partial x_j} \right) + \frac{\partial}{\partial t} \left( [\rho (u_j - v_j) + \rho_0 v_j] \frac{\partial H}{\partial x_j} \right) \end{aligned} \quad (2.22)$$

where  $H$  is still the Heaviside function. This formulation does take the aspect of source motion into account. However, in many cases it is also convenient to use a reference moving with the source. This would resemble a windtunnel setup or microphones traveling with the source through a flow field. With this assumption the Fflowcs Williams and Hawkins equation will take the following form

$$\left\{ \frac{\mathbf{D}_\infty^2}{\mathbf{D}t^2} - c_\infty^2 \frac{\partial^2}{\partial x_i^2} \right\} \rho' H = \frac{\partial^2}{\partial x_i \partial x_j} [T_{ij} H] + \frac{\partial}{\partial x_i} [F_i \delta(f)] + \frac{\partial}{\partial t} [Q \delta(f)] \quad (2.23)$$

where the quadropole, dipole and monopole sources are on the form,

$$T_{ij} = \rho (u_i - U_i^\infty) (u_j - U_j^\infty) (p - c_\infty^2 \rho') \delta_{ij} - \tau_{ij}, \quad (2.24)$$

$$F_i = - \left[ \rho (u_i - 2U_i^\infty) u_j + \rho_\infty U_i^\infty U_j^\infty + p \delta_{ij} - \tau_{ij} \right] \frac{\partial f}{\partial x_j}, \quad (2.25)$$

$$Q_i = [\rho u_i - \rho_\infty U_i^\infty] \frac{\partial f}{\partial x_j}. \quad (2.26)$$

When expressing the equation in a moving frame of reference, Fourier transform can be used to transform the equation into frequency domain<sup>30</sup>,

$$\begin{aligned} & \left\{ \frac{\partial^2}{\partial x_i^2} + k^2 - 2iM_i k \frac{\partial}{\partial x_i} - M_i M_j \frac{\partial^2}{\partial x_i \partial x_j} \right\} c_\infty^2 \hat{\rho} H = \\ & \frac{\partial^2}{\partial x_i \partial x_j} [T_{ij} H] + \frac{\partial}{\partial x_i} [F_i \delta(f)] + \frac{\partial}{\partial t} [Q \delta(f)]. \end{aligned} \quad (2.27)$$

This formulation is related to Equation (2.11) and the Green's functions can be used to retrieve a solution. The sources in Equation (2.27) are then described by

$$T_{ij} = \rho (u_i - U_i^\infty) (u_j - U_j^\infty) (p - c_\infty^2 \rho) \delta_{ij} - \tau_{ij}, \quad (2.28)$$

$$F_i = - \left[ \rho (u_i - 2U_i^\infty) u_j + p \delta_{ij} - \tau_{ij} \right] n_j, \quad (2.29)$$

$$Q_i = \rho u_i n_i. \quad (2.30)$$

## 2.5 Vortex Sound

Powell formulated an aeroacoustic analogy which highlights the significance of vorticity as an acoustic source<sup>10</sup>. In this formulation the Lamb vector,  $\mathbf{L} = (\boldsymbol{\omega} \times \mathbf{u})$ , acts as a source, where  $\mathbf{u}$  is the velocity vector and  $\boldsymbol{\omega}$  is the vorticity vector. The vorticity based formulation can have the advantage in that the source region can be less geometrically extended than the source region from Lighthill's analogy. This would mean that a smaller region of the flow would have to be used to evaluate the aeroacoustic sources. The derivation of this analogy starts at the flow equations, but with the vorticity introduced as a variable by using,  $\boldsymbol{\omega} = \nabla \times \mathbf{u}$ , and the vector identity

$$\frac{1}{2}\nabla(\mathbf{u} \cdot \mathbf{u}) = \mathbf{u} \times (\nabla \times \mathbf{u}) + (\mathbf{u} \cdot \nabla)\mathbf{u}. \quad (2.31)$$

The momentum equation given in Equation (2.2) will have the form

$$\rho \frac{\partial \mathbf{u}}{\partial t} + \nabla(p + \frac{1}{2}\rho|\mathbf{u}|^2) + \rho(\boldsymbol{\omega} \times \mathbf{u}) + \nabla \cdot \boldsymbol{\tau} = 0. \quad (2.32)$$

Using a similar manipulation as for Lighthill's analogy, taking the time derivative of Equation (2.1) and add that to the spatial derivative to Equation (2.32), the following is retrieved

$$\frac{1}{c_0^2} \frac{\partial^2 p'}{\partial t^2} - \frac{\partial^2 p'}{\partial x_i^2} = \nabla \cdot \left[ \rho(\boldsymbol{\omega} \times \mathbf{u}) + \nabla \left( \frac{1}{2}\rho|\mathbf{u}|^2 \right) - \mathbf{u} \frac{\partial \rho}{\partial t} - \frac{1}{2}|\mathbf{u}|^2 \nabla \rho \right] + \frac{\partial^2}{\partial t^2} \left( \frac{p'}{c_0^2} - \rho' \right) \quad (2.33)$$

For isentropic flow at low Mach numbers the RHS may be approximated by,

$$\frac{1}{c_0^2} \frac{\partial^2 p'}{\partial t^2} - \frac{\partial^2 p'}{\partial x_i^2} = \nabla \cdot [\rho(\boldsymbol{\omega} \times \mathbf{u})], \quad (2.34)$$

giving the Lamb vector as the source of sound for these conditions.

Howe furthermore derived a vortex-based analogy with the total enthalpy as the acoustic variable.

$$B = \int \frac{dp}{\rho} + \frac{1}{2}\mathbf{u}^2 \quad (2.35)$$

This will result in an analogy that naturally relates to a potential flow rather than the free field used in Lighthill's analogy. The total enthalpy is introduced by considering the momentum equation in Crocco's form

$$\frac{\partial \mathbf{u}}{\partial t} + \nabla B = -\boldsymbol{\omega} \times \mathbf{u} \quad (2.36)$$

and subtracting the divergence of the momentum equation from the time derivative of the continuity equation, in a similar way as Lighthill's analogy. And by assuming a high Reynolds number homentropic flow, neglecting viscous dissipation, the following vortex sound equation is attained

$$\left( \frac{D}{Dt} \left( \frac{1}{c^2} \frac{D}{Dt} \right) - \frac{1}{\rho} \nabla \cdot (\rho \nabla) \right) B = \frac{1}{\rho} \nabla \cdot (\rho \boldsymbol{\omega} \times \mathbf{u}). \quad (2.37)$$

In steady irrotational regions, fluctuations in the total enthalpy can then be related to the velocity potential,  $B = -\partial\phi/\partial t$ . For this case the Lamb vector also becomes the important source term. However, compared to the formulation by Powell this formulation incorporates the effect of a potential flow for the wave equation.

Howe further showed that for low Mach numbers the wave operator may be simplified, as  $c = c_0$  and  $\rho = \rho_0$  is the far-field speed of sound and density. Also, by neglecting the nonlinear effects of propagation and scattering of sound by vorticity. The pressure at a receiver located in the far-field may then be described by the approximation,  $p \approx \rho_0 B$ .

## 2.6 Conclusions

The aeroacoustic analogies presented in this chapter are all derived based on the flow equations. Depending on the assumptions made and choice of acoustic variable, these will take very different forms. It is therefore important to consider which assumptions need to be made in the analogies, in order to find a formulation that is suitable. Considerable simplifications can also be made to the source formulation by assuming that some terms are small. For example, by assuming a low Mach number or that no chemical reactions are occurring. Without making assumptions, the solution will not be much easier than a direct simulation.



# 3

## The Wave Expansion Method

The Wave Expansion Method (WEM) is a discretization technique that can be used for harmonic wave propagation problems. Common examples of these types of problems are finding solutions to the Helmholtz equation, the convected form of the Helmholtz equation or the Linearized Euler equations. To solve these types of wave propagation problems for a longer distance, with regard to wavelength, is often challenging. This is since the computational domain, in terms of discretization points, will become quite large. To minimize the computational cost, it is therefore essential to have a numerical method that is efficient in terms of points per wavelength. More specifically, it is significant that the dispersion or phase errors are small for wave propagation problems. The formulation in the WEM possesses this quality, using natural waves or Green's functions of plane waves in the discretization procedure. It is therefore well suited for these harmonic propagation problems solved in frequency domain.

Many volume discretizing schemes like the FDM or the FEM have a dependence on the type of elements or structure of the grid used for the computations. In the WEM, the elements are only used to find the neighbours of the nodes. Therefore, the form or shape of the elements is more or less arbitrary. This also means that the difference in programming effort is quite similar in one-, two- or three-dimensions. This close to mesh-less property is elaborated on in Paper B and in Chapter 5.

In the following sections, the discretization and setting up of standard boundary conditions is shown. Further descriptions of this discretization is also found in Caruthers et. al.<sup>20</sup> or Ruiz and Rice<sup>23</sup>.

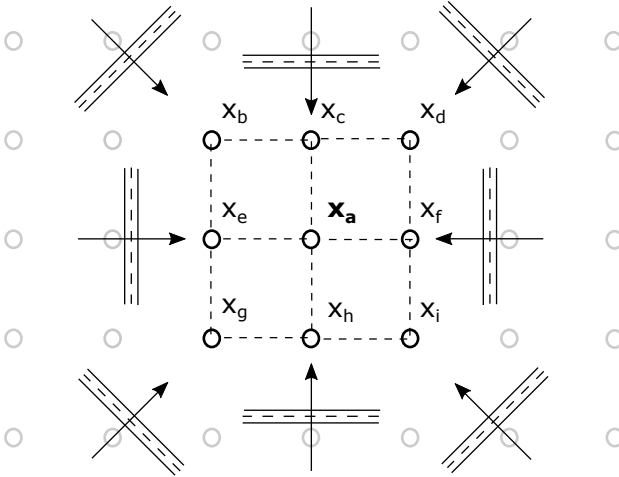


Figure 3.1. Schematic sketch of WEM discretization.

### 3.1 Discretization

A schematic of the discretization in WEM is shown in Figure 3.1. This figure shows the center-node, at a location referred to as  $\mathbf{a}$ , and surrounding nodes, at locations referred to as  $\mathbf{b-f}$ , which are connected using square elements. A number of incoming plane waves are also illustrated surrounding these nodes. The directions of these plane-waves are evenly distributed around the nodes, and the number of waves does not have to correspond to the number of surrounding nodes.

Using the discretization for a harmonic variable  $\phi$ , the variable  $\phi$  at  $\mathbf{x}_a$  can be approximated by a superposition of acoustic fields which are defined by a number of  $J$  plane waves. These plane-waves have the amplitude  $\gamma_j$  and direction vector  $\alpha_j$ . The unknown,  $\phi$ , at  $\mathbf{x}_a$  can thereby be described by

$$\phi_a = \sum_{j=1}^J \gamma_j e^{-i\mathbf{k}\alpha_j \cdot \mathbf{x}_a}. \quad (3.1)$$

To simplify the notation a vector,

$$\mathbf{h}_a = \left[ e^{-i\mathbf{k}\alpha_1 \cdot \mathbf{x}_a} \ e^{-i\mathbf{k}\alpha_2 \cdot \mathbf{x}_a} \ \dots \ e^{-i\mathbf{k}\alpha_J \cdot \mathbf{x}_a} \right], \quad (3.2)$$

is used to describe the plane-waves and a vector,

$$\boldsymbol{\gamma} = [\gamma_1 \ \gamma_2 \ \dots \ \gamma_J]^T, \quad (3.3)$$

contains the amplitudes of these waves. Thus, the shorter notation becomes

$$\phi_a = \mathbf{h}_a \boldsymbol{\gamma}. \quad (3.4)$$

$\phi$  at the neighbouring nodes is then approximated by the same waves given by

$$\boldsymbol{\phi}_{nb} = \mathbf{H} \boldsymbol{\gamma} \quad (3.5)$$

where

$$\boldsymbol{\phi}_{nb} = [\phi_b \ \phi_c \ \phi_d \ \phi_e \ \phi_f \ \phi_g \ \phi_h \ \phi_i]^T \quad (3.6)$$

and

$$\mathbf{H} = [\mathbf{h}_b^T \ \mathbf{h}_c^T \ \mathbf{h}_d^T \ \mathbf{h}_e^T \ \mathbf{h}_f^T \ \mathbf{h}_g^T \ \mathbf{h}_h^T \ \mathbf{h}_i^T]^T \quad (3.7)$$

When the number of plane waves are larger than the number of neighbouring nodes the system is under-determined. This local system of equations is then solved and the waves amplitudes are calculated by premultiplying with the Moore-Penrose pseudo-inverse of  $\mathbf{H}$ .

$$\boldsymbol{\gamma} = \mathbf{H}^+ \boldsymbol{\phi}_{nb} \quad (3.8)$$

By introducing this into Equation (3.4), the variable  $\phi$  at  $\mathbf{x}_a$  can be related to  $\phi$  at the neighbouring nodes as,

$$\phi_a = \mathbf{h}_a \mathbf{H}^+ \boldsymbol{\phi}_{nb}. \quad (3.9)$$

As this procedure is performed for each node in the computational domain, a system of equations in the form of Equation (3.10) can be assembled as

$$\mathbf{K} \boldsymbol{\phi} = \mathbf{Q}. \quad (3.10)$$

Where  $\mathbf{K}$  is an unsymmetric and sparse system matrix which will be the discretized wave operator, and  $\mathbf{Q}$  is a vector where sources can be added.

## 3.2 Planewave formulations

The acoustic waves used in the WEM discretization are based on plane-wave solutions to the harmonic propagation equation of interest. These plane-waves will have the form

$$\phi = \mathbf{v} e^{ik \cdot \mathbf{x}} \quad (3.11)$$

where  $\mathbf{v}$  is the eigenvector and  $k$  is the wave number. If we consider the Helmholtz equation given by

$$\left\{ \nabla^2 + \frac{\omega^2}{c^2} \right\} \phi = 0, \quad (3.12)$$

where  $c$  is the speed of sound and  $\omega$  the angular frequency. Then insert the plane-wave solution from Equation (3.11) into Equation (3.12), this will result in a characteristic equation on the form,

$$-k^2 \mathbf{v} e^{-ik(\boldsymbol{\theta} \cdot \mathbf{x})} + \frac{\omega^2}{c^2} \mathbf{v} e^{-ik(\boldsymbol{\theta} \cdot \mathbf{x})} = 0, \quad (3.13)$$

where  $\boldsymbol{\theta}$  is the wave direction vector. For this case  $\mathbf{v} = 1$ , and the equation can be solved giving the wave numbers

$$k^{(1)} = \frac{\omega}{c} \quad k^{(2)} = -\frac{\omega}{c} \quad (3.14)$$

In the case of a mean flow the convected form of the Helmholtz equation is

$$\left\{ \nabla^2 - \left( \frac{1}{c} \mathbf{u} \cdot \nabla \right)^2 - \frac{2i\omega}{c^2} \mathbf{u} \cdot \nabla + \frac{\omega^2}{c^2} \right\} \phi = 0. \quad (3.15)$$

which together with Equation (3.11) gives the characteristic equation

$$\left( 1 - \left( \frac{1}{c} \mathbf{u} \cdot \boldsymbol{\theta} \right)^2 \right) k^2 - \frac{2\omega}{c^2} \mathbf{u} \cdot \boldsymbol{\theta} k + \frac{\omega^2}{c^2} = 0. \quad (3.16)$$

Solving this equation for the wavenumbers gives

$$k^{(1)} = \frac{\omega}{\mathbf{u} \cdot \boldsymbol{\theta} + c} \quad k^{(2)} = -\frac{\omega}{\mathbf{u} \cdot \boldsymbol{\theta} - c} \quad (3.17)$$

Systems of equation can also be solved, introducing more variables by for example coupling the linearized mass and momentum equations.

$$i\omega \hat{p} + \rho c^2 \nabla \cdot \hat{\mathbf{u}} = 0 \quad (3.18)$$

$$i\omega \hat{\mathbf{u}} + \frac{1}{\rho} \nabla \hat{p} = 0 \quad (3.19)$$

Solving the characteristic equation for this system of equations gives the wave number,

$$k^{(1)} = \frac{\omega}{c} \quad k^{(2)} = -\frac{\omega}{c}, \quad (3.20)$$

and the eigenvectors

$$\mathbf{v}^{(1)} = \begin{bmatrix} 1 \\ \theta_x/(\rho c) \\ \theta_y/(\rho c) \\ \theta_z/(\rho c) \end{bmatrix} \quad \mathbf{v}^{(2)} = \begin{bmatrix} -1 \\ \theta_x/(\rho c) \\ \theta_y/(\rho c) \\ \theta_z/(\rho c) \end{bmatrix} \quad (3.21)$$

The eigenvectors and wavenumbers for the desired propagation equations are then used in the discretization procedure of the WEM as described previously.

### 3.3 Boundary conditions

#### 3.3.1 Dirichlet

The Dirichlet boundary condition for the  $n^{\text{th}}$  node is enforced by setting the non-zero position  $\mathbf{K}(n, n)$  of the system matrix to one and the corresponding position of the source vector  $\mathbf{Q}(n)$  to the boundary condition value.

#### 3.3.2 Neumann

A Neumann condition is imposed by augmenting the gradient condition to Equation (3.5) for the nodes on the boundary as,

$$\begin{bmatrix} \phi_{nb} \\ \mathbf{v}_n \end{bmatrix} = \begin{bmatrix} \mathbf{H} \\ \mathbf{n} \cdot \nabla \mathbf{h} \end{bmatrix} \boldsymbol{\gamma} = \mathbf{H}_{aug} \boldsymbol{\gamma}, \quad (3.22)$$

where  $\mathbf{v}_n$  is the wall velocity and has the same number of entries as the number of nodes of the stencil that are on the boundary.  $\mathbf{n}$  is the normal unit vector. The derivative is evaluated by setting

$$\mathbf{n} \cdot \nabla h_j = ik(\mathbf{n} \cdot \boldsymbol{\alpha}_j)h_j \quad (3.23)$$

The pseudo-inverse of  $\mathbf{H}_{aug}$  is

$$\boldsymbol{\gamma} = \left[ \mathbf{H}_{aug}^+ \right] \begin{bmatrix} \phi_{nb} \\ \mathbf{v}_n \end{bmatrix}, \quad (3.24)$$

and Equation (3.9) then becomes

$$\phi_a - \mathbf{h} \mathbf{H}_{aug,L}^+ \phi_{nb} - \mathbf{h} \mathbf{H}_{aug,R}^+ \mathbf{v}_n = 0, \quad (3.25)$$

where  $\mathbf{H}_{aug,L}^+$  contains the first  $J$  columns of  $\mathbf{H}_{aug}^+$ , and  $\mathbf{H}_{aug,R}^+$  contains the columns corresponding to the boundary nodes. For non-zero entries of  $\mathbf{v}_n$  the part  $\mathbf{h} \mathbf{H}_{aug,R}^+ \mathbf{v}_n$  is added to the source vector  $\mathbf{Q}$ .

#### 3.3.3 Radiation

A non-reflecting boundary condition can be implemented in the WEM by only considering plane waves traveling out of the domain. For the interior nodes described in Figure 3.1, the plane waves should have a uniform distribution surrounding the node which is evaluated. However, a non-reflecting boundary condition can

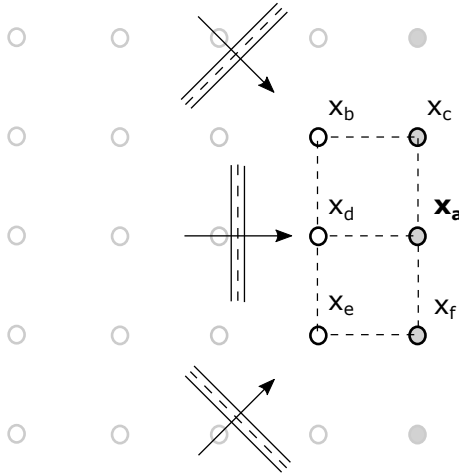


**Figure 3.2.** Schematic sketch of point source WEM discretization.

be achieved by only directing these waves out of the domain, preventing the waves from travelling in the opposite direction. In this work the outgoing waves are distributed between an angle of 45 degrees from the boundary's local normal vector, illustrated in Figure 3.2. The treatment at the outer boundaries is discussed further in Ruiz and Rice<sup>23</sup>.

# 4

## Introduction of sources

This chapter describes the procedure to include sources in the WEM. To demonstrate the use of the solution procedure with distributed sources, some well defined test cases are used. These cases highlight the efficiency and possibility to use the method. The test cases considered are well known and can for some cases be compared to analytical solutions. This is convenient since the error can be easily evaluated. The chapter should be regarded as an extended summary of Paper A.

### 4.1 Point sources

Point sources need special consideration in the WEM. A robust way to introduce a point monopole source in the Helmholtz equation was introduced by Liu<sup>27</sup>, where the point source was distributed to the neighbouring nodes using free field Green's functions. Given the stencil in Figure 4.1, the pressure at a node at location  $\mathbf{x}_1$  from a monopole source at a node located at  $\mathbf{x}_s$  can be evaluated using a Green's function. The pressure in the node located at  $\mathbf{x}_1$  is then formulated as

$$\phi_1 = \mathbf{h}_1 \boldsymbol{\gamma} + q \quad (4.1)$$

where  $q$  is a monopole source contribution,

$$q = i\omega\rho_0 Q_s G(\mathbf{x}_1 | \mathbf{x}_s). \quad (4.2)$$

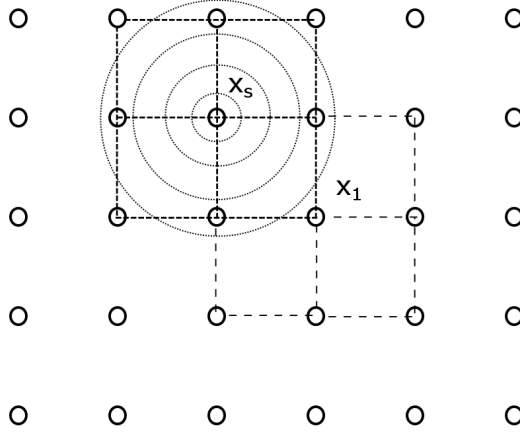


Figure 4.1. Point source discretization stencil.

$G$  corresponds to the Green's function,  $\omega$  is the frequency,  $Q_s$  is the source strength and  $\rho_0$  is the density. As described previously, the pressure at the neighbouring nodes are included through

$$\phi_n = \mathbf{h}_n \gamma + \mathbf{Q}_1 \quad (4.3)$$

where  $\mathbf{Q}_1$  is the source distribution at the corresponding nodes evaluated with the Green's function

$$\mathbf{Q}_1 = i\omega\rho_0 Q_s \mathbf{G}(\mathbf{x}_n | \mathbf{x}_s) \quad (4.4)$$

Since the solution is not given at the source node, this node is left out from the evaluation at node 1. This gives the following expression for the pressure in node 1,

$$\phi_1 - \mathbf{h}_1 \mathbf{H}_n^+ \phi_n = q - \mathbf{h}_1 \mathbf{H}_n^+ \mathbf{Q}_1 \quad (4.5)$$

In a similar fashion the Green's function of a multipole source can be introduced. For a monopole the free-field Green's function in 2D, as described in Chapter 3, is

$$G(\mathbf{x}, \mathbf{x}_0) = \frac{-i}{4} H_0^{(2)}(k|\mathbf{x} - \mathbf{x}_0|) \quad (4.6)$$

where  $H_0^{(2)}$  is the zeroth order Hankel function of the second kind,  $k$  is the wave number and  $\mathbf{x}$  the location of the receiver.

For a dipole source the resulting derivative of the Green's function is given by

$$\frac{\partial G}{\partial x} = \frac{-ik}{4} H_1^{(2)}(k|\mathbf{x} - \mathbf{x}_0|) \quad (4.7)$$

Here  $H_1^{(2)}$  is the first order Hankel function of second kind. For a dipole source  $q$  will represent a force, also giving it the directivity. The pressure for a monopole and dipole point source in a free-field, computed on three different grid levels, is compared to the analytical solution in Figure 4.2. The computed solutions gives a perfect match to the analytical solution. By adding yet another derivative to the Green's function a quadropole source can also be achieved in the same way. As described in chapter 2, Prandtl-Glauert transformation can be used to include the effect of a mean flow in the Green's function.

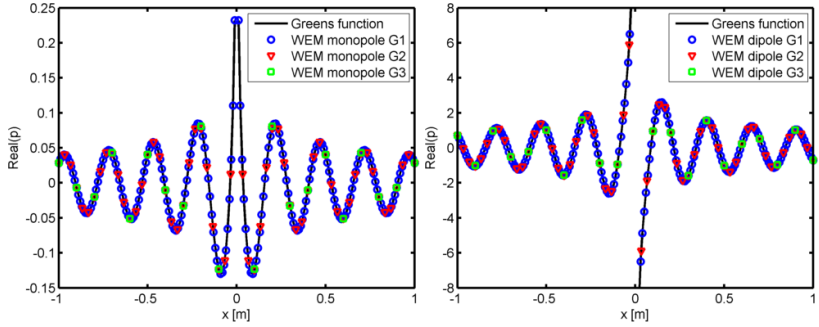


**Figure 4.2.** Pressure of a dipole and monopole point source computed at grid level G1, G2 and G3.

## 4.2 Distributed CFD sources

The sources based on the aeroacoustic analogies from Chapter 2 consist of spatially distributed variables. To use the source introduction method described previously, this distributed source is described by a cloud of point sources, where each CFD cell corresponds to one point source. This is achieved by performing a spatial integration of the source variable in each CFD cell and then introducing each of these as point sources on the acoustic grid. The point sources are introduced on the nearest node and its surrounding as illustrated in Figure 4.3. Using Equation (4.1) and the stencil in Figure 3.1, the variable  $\phi$  on a surrounding acoustic node to a quadropole source is given by

$$\phi_1 = \mathbf{h}_1 \boldsymbol{\gamma} + q \quad (4.8)$$

where

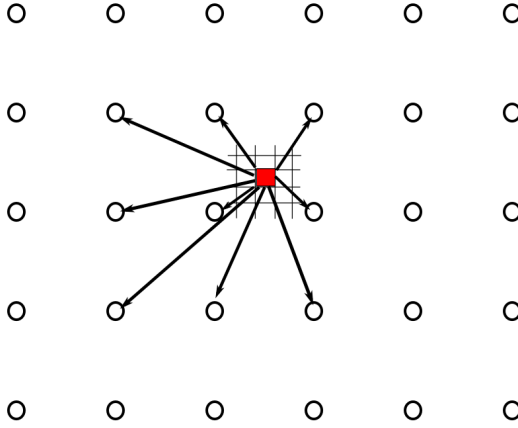


**Figure 4.3.** Schematic sketch of CFD to WEM source introduction. The red square on the fine CFD mesh is introduced on the nodes on the acoustic grid which is marked by circles.

$$q = Q_s \frac{\partial^2}{\partial x_i \partial x_j} G(\mathbf{x}_1 | \mathbf{x}_s) \quad (4.9)$$

and  $Q_s$  is the quadrupole strength, corresponding to the aeroacoustic source integrated over a CFD cell. All the CFD cells are then introduced on the acoustic grid in order to transfer the sources to the acoustic grid.

### 4.3 Co-rotating vortex pair

A case of a co-rotating vortex pair is used to evaluate the previously defined implementation for sources that are described by a flow field. The vortex-pair has been used numerous times for the validation and investigation of aeroacoustic methods. The flow field consists of two thin line-vortices that imposes a rotation on each other. As the two rotate around each other, an acoustic field similar to that of a rotating quadrupole is generated. In the following section the acoustic field by these vortices is computed with sources described by both Lighthill's analogy and the Vortex Sound Theory. The computed sound fields are then compared to an analytical solution given by Howe<sup>11</sup>.

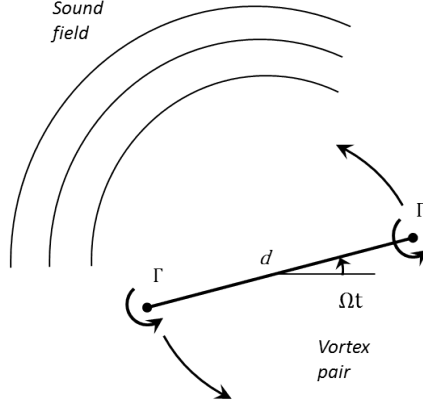


Figure 4.4. Co-rotating vortex pair sound generation, Howe<sup>11</sup>.

### 4.3.1 Analytical solution

Assuming a low Mach number flow, each of the two vortices can be described by a Lamb-Oseen vortex, see Saffman<sup>31</sup>. The mathematical description in terms of velocity of such a vortex is,

$$u_1 = -u_\Theta \frac{y_2 - y_2^0}{r_y}; \quad u_2 = -u_\Theta \frac{y_1 - y_1^0}{r_y}; \quad u_\Theta = \frac{\Gamma}{2\pi r_y} (1 - e^{-r_y^2/2\sigma^2}), \quad (4.10)$$

where  $u_1$ ,  $u_2$  and  $u_\Theta$  are the velocity components;  $y_1$  and  $y_2$  are the spatial coordinates;  $y_1^0$  and  $y_2^0$  are the coordinates for the vortex origin;  $r_y$  is the radius from the vortex core;  $\Gamma$  is the circulation and  $\sigma$  is a parameter that determines the size of the vortex core. The vorticity,  $\omega$ , of each vortex can then be described by

$$\omega = \frac{\Gamma}{2\pi\sigma^2} e^{-r_y^2/2\sigma^2}. \quad (4.11)$$

As presented by Howe<sup>11</sup>, there exists an analytical solution for the radiated sound at a position,  $\mathbf{x}$ , in the acoustic far-field generated by the co-rotating vortices. By assuming that the source is compact with regard to the acoustic wavelength the pressure is given by,

$$p'(\mathbf{x}) \approx -4 \sqrt{\frac{\pi d}{2r}} \rho_0 U^2 M^{\frac{3}{2}} \cos \left[ 2\varphi - 2\Omega \left( t - \frac{r}{c_0} \right) + \frac{\pi}{4} \right], \quad (4.12)$$

where  $d$  is the distance between the vortices,  $r$  is the distance from the center of rotation to the listener position,  $\varphi$  is the angle,  $\rho_0$  is the density,  $U$  the rotation

velocity,  $M$  is the rotation Mach number,  $c_0$  is the speed of sound,  $\Omega$  is the angular frequency and  $t$  is the time. The existence of analytical solutions for both the flow and acoustic field makes the co-rotating vortex case very convenient for validation of numerical methods.

### 4.3.2 Numerical solution

Two different regions are considered in the computation of this case. One contains the flow solution,  $\Omega_f$ , which is given from the analytical description. The other covers the acoustic part of the domain,  $\Omega_a$ . The acoustic region is significantly larger than the flow domain in the setup considered, since the source is compact with regard to the wavelength and it is desired to perform the computations on a domain that covers at least a number of wavelengths. A free-radiation boundary condition is imposed at the outer perimeter of  $\Omega_a$  to avoid reflections of the acoustic waves propagating out of the domain. The different regions used are illustrated in Figure 4.5.

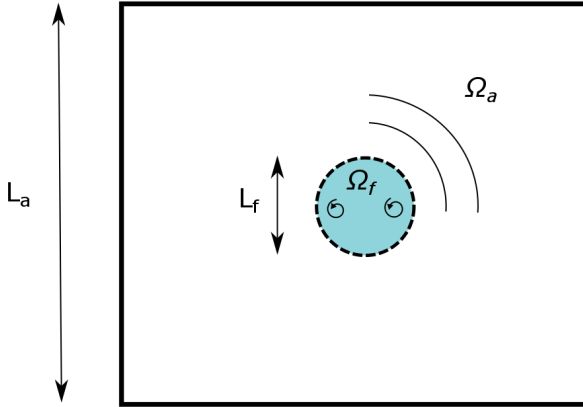


Figure 4.5. Co-rotating vortex pair domains.

By assuming the flow to be at rest, the inhomogeneous Helmholtz equation for the acoustic propagation based on the aeroacoustic analogies will be

$$(\nabla^2 + k^2)\hat{p} = \hat{s} \quad \mathbf{x} \in \Omega = \Omega_f \cup \Omega_a \quad (4.13)$$

where  $k$  is the wave number and  $\hat{s}$  is the source in frequency domain. In the flow domain,  $\Omega_f$ , the aeroacoustic sources are computed at each node using both

Powell's and Lighthill's aeroacoustic analogies. Powell's analogy will give volume sources related to the vorticity, in the form

$$s = \nabla \cdot [\rho_0(\boldsymbol{\omega} \times \mathbf{u})], \quad (4.14)$$

where  $\mathbf{u}$  is the velocity vector,  $\boldsymbol{\omega}$  is the vorticity vector and  $\rho_0$  is the farfield density. The quadropole source in Lighthill's formulation will give the following volume source term,

$$s = \frac{\partial^2}{\partial x_i \partial x_j} T_{ij}. \quad (4.15)$$

The sources are evaluated in time domain and then transformed to frequency domain. In  $\Omega_a$ , the source term,  $\hat{s}$ , is set to zero.

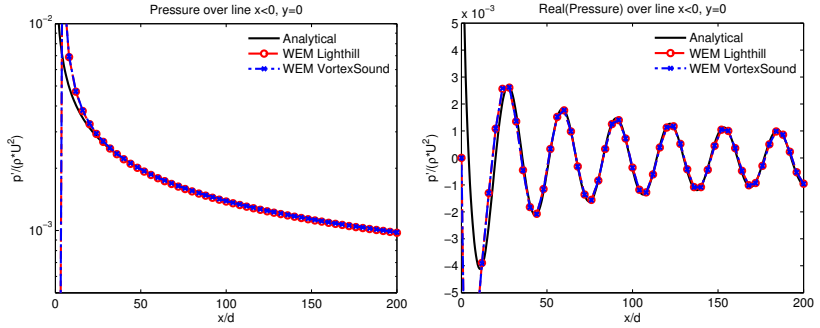


**Figure 4.6.** Pressure at the rotation frequency, presented on a line from the center of the domain to the outer boundary for the solutions based on; the analytical expression; Lighthill analogy and Vortex sound analogy. Left: pressure real part; right: pressure amplitude.

For the computations, the acoustic region was set to a width of  $L_a = 400d$  and the diameter of the source region was equal to,  $L_f = 2d$ . Both domains were discretized using equally spaced square elements, 40000 node in the acoustic grid and 2500 nodes in the flow grid. The circulation of a vortex pair is described by,  $\omega = 2U/d = \Gamma/(\pi d^2)$ . For the considered case, the Mach number,  $M = U/c$  was equal to  $M = 0.05$ , where  $U$  is the rotational velocity and  $c$  is the speed of sound.

In Figure 4.6, the pressure on a line from the center of rotation is presented and the numerical solutions of the analogies are compared to the analytical solution. Close to the centre of rotation in the near field the solutions tend to differ, which is expected since the analytical solution is not valid in this region. However, if we consider the region at about one wavelength from rotational centre, then the solutions converge towards the same pressure.

Considering the two analogy formulations there is more or less no difference in the results, although the formulation of the sources is quite different. Lighthill's

analogy uses a quadrupole formulation of the volume sources, while Powell's analogy uses a dipole formulation. The results should of course agree for this case, although the implementation of the sources becomes different. Therefore, it shows that the numerical implementation is working with both quadrupoles and dipoles. However, even though they produce similar results in a case such as this one, with perfect analytical description of the source, they might still show different sensitivity to errors that might occur in this description. This has previously been highlighted by Martínez-Lera et. al.<sup>12</sup>. The vortex sources then appeared to be much more sensitive to an artificial error that was introduced on top of the sources. The sensitivity was considered to be connected to the dipole formulation in this analogy.

#### 4.4 Cylinder in cross-flow

In this section, a cylinder in flow conditions corresponding to three different Mach numbers is considered. The dimensions of the cylinder are scaled to give a Reynolds number of  $Re=150$ . At these conditions the flow is dominated by a periodic shedding from the upper and lower side. The vortices shed are then transported downstream by the mean flow, resulting in a very extended wake region. The strong periodic shedding also generates an acoustic field similar to that of a dipole. Strong sound fields generated by shedding of vortices behind cylinders usually have a distinct tonal behaviour, which is referred to as aeolian sound. As the Mach number increases this sound field is also influenced by quadrupole sources and mean flow effects. For the acoustic propagation solution to capture this field correctly, both the convective effects of the flow and the quadrupole sources in the wake need to be included. This makes it a more challenging case than the co-rotating vortex pair.

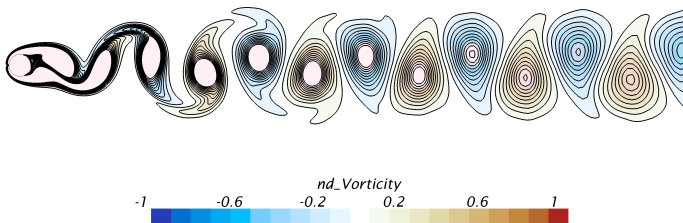


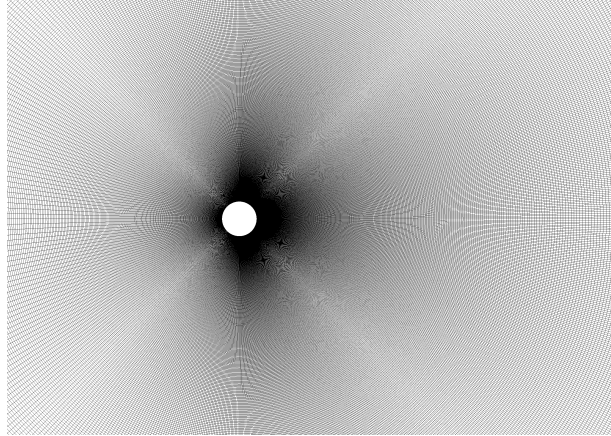
**Figure 4.7.** Contour of non-dimensional vorticity.

**Table 4.1.** Cylinder flow domain grid parameters.

	Radial nodes	Circumferential nodes	Total nodes
Coarse	360	300	108,000
Medium	460	400	184,000
Fine	840	800	588,000

#### 4.4.1 Flow solution

The cylinder flow field was simulated using the Star-CCM+ v10.02 commercial flow solver. Three different flow conditions were considered,  $M_\infty=0.1$ ,  $M_\infty=0.2$  and  $M_\infty=0.3$ , where  $M_\infty$  is the free-stream Mach number. The dimensions of the cylinder and flow properties were set to give a Reynolds number of  $Re=150$ ,  $Re = LU/\nu$ , where  $L$  is the diameter of the cylinder,  $U$  the free-stream velocity and  $\nu$  is the dynamic viscosity. At this Reynolds number the flow around the cylinder can be considered two-dimensional. The 2D assumption is valid for a Reynolds number lower than  $Re = 200$ . However, at higher Reynolds numbers the vortex structures are known to form in three dimensions. 3D simulations are then needed to capture the flow properly. Due to the low Reynolds number, the computations were performed without a turbulence model and considered as laminar. 2<sup>nd</sup>-order numerical schemes were used for both time and space, with a sufficiently small time-step to resolve all the relevant properties. Three different grid levels were also used to evaluate the grid convergence of the solutions. The different grids are summarized in Table 4.1 and a close up of the grid close to the cylinder is shown in Figure 4.8.

**Figure 4.8.** Close-up near the cylinder of the finest grid used in the CFD computations.

**Table 4.2.** Cylinder forces in relation to previous publications.

Reference	$Re$	$C_L(RMS)$	$C_D$
Current study at Mach=0.1	150	1.32	0.368
O. Posdziecha, R. Grundmannb, 2007	150	1.299	0.356
L. Qu, C Norberg L. Davidson et. al., 2013	150	1.303	0.355
Park, 1998	150	1.32	0.364

At the Reynolds number considered, the flow around the cylinder is dominated by a two-dimensional periodic vortex shedding. The vortices shed from the cylinder are convected downstream by the mean flow and form what is usually referred to as a Von Karman vortex sheet. These vorticity structures downstream the cylinder are shown in Figure 4.7 using vorticity contours at a single time-step. The oscillating flow caused by cylinders at Reynolds number,  $Re=150$ , has been the subject of numerous numerical and experimental investigations, see e.g. Qu et.al<sup>32</sup>, Park et.al<sup>33</sup> and Williamson et.al<sup>34</sup>, where the reduced frequency,  $k = 2\pi L/U_\infty$ , predicted for the vortex shedding ranges from  $0.57 < k < 0.58$ . The frequency range computed for the different grid levels and Mach numbers in this study was  $0.57 < k < 0.58$ . The drag and lift force acting on the cylinder was predicted in the range  $1.31 < C_D < 1.37$  and  $0.36 < C_L(RMS) < 0.38$ . Both the drag and lift force showed an increasing trend with increasing Mach number. All these results are considered to be in good agreement with previously published results presented in Table 4.2.

#### 4.4.2 Acoustic solution

The acoustic analogy used to solve the acoustic propagation of this case is a frequency formulation of the Ffowcs Williams and Hawkings equation described in section 2.4. This formulation is based on a windtunnel type of setup, where the object is seen as stationary in a moving flow. This is convenient since it resembles the setup in the flow computation. In this aeroacoustic analogy the convection of the flow is included in the wave operator, leading to a source formulation where the convection of the flow is deducted from the volume sources. The source terms will therefore have the following form,

$$T_{ij} = \rho(u_i - U_i^\infty)(u_j - U_j^\infty) + (p - c_\infty^2 \rho)\delta_{ij} - \tau_{ij}, \quad (4.16)$$

$$F_i = (p\delta_{ij} - \tau_{ij})n_j, \quad (4.17)$$

where  $U^\infty$  is the free stream convection velocity,  $u$  is the velocity,  $\rho$  is the density,  $c_\infty$  is the speed of sound,  $p$  is the pressure and  $\tau_{ij}$  is the viscous stress tensor. These sources are computed and evaluated from the CFD solution for a time series, which is then transformed into frequency domain using Fast Fourier Transform(FFT).

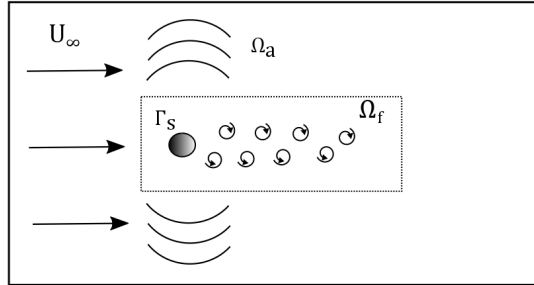


**Figure 4.9.** Domains used for the acoustic computation.

The domain used for the acoustic computation is illustrated in Figure 4.9.  $\Omega_f$  is a region where the sources are evaluated from the flow simulation. In the region outside,  $\Omega_a$ , the source is equal to zero and the propagation is governed by the convected Helmholtz equation. The surface,  $\Gamma_s$ , is included in the acoustic region. On this surface the dipole sources based on the pressure on the surface of the cylinder are introduced. This problem setup will therefore correspond more to a radiation problem, which could be solved using integral methods mentioned earlier. However, it also shows that the sources are transferred to the acoustic propagation solution, which is the goal. For future simulations the target is to include the scattering of the walls by using a Neumann boundary condition instead of using the dipoles to include this part.

Since the compressible flow equations are solved, the acoustic pressure can be extracted directly from the CFD solution. The solution accuracy will deteriorate with the distance from the cylinder due to the coarser grid in the outer regions of the domain. Dispersion and dissipation errors will then have a significant impact on the acoustic waves. However, while remaining in the region close to the cylinder, the CFD solution is still considered to satisfactorily capture the acoustic field. The ability to capture the acoustic waves is of course also related to the wavenumber. With higher Mach number the wavenumber is increased and more grid points would be needed to properly resolve the acoustic waves. For the cases considered, the solution is regarded to give reasonable accuracy up to  $20d$  for all Mach numbers.

The acoustic field generated around the cylinder is dominated by the shedding

frequency and the harmonics of this tone. The frequency spectra of the pressure at two points, one at a location  $20 d$  perpendicular to the cylinder and one  $20 d$  upstream of the cylinder is presented in Figure 4.10 together with the time signal. The shedding frequency and its harmonics appears as distinct peaks in the spectra at the perpendicular location. The peak at shedding frequency is not predicted in the upstream location. However, the first harmonic is predicted higher at this location. This reveals some of the directivity of the source. The shedding frequency, which is related to the lift force fluctuations gives a strong perpendicular directivity. While the first harmonic is connected to the drag force, resulting in a stronger upstream directivity.

With this tonal behaviour taken in to consideration, the acoustic evaluation is performed at this shedding frequency and its harmonics.

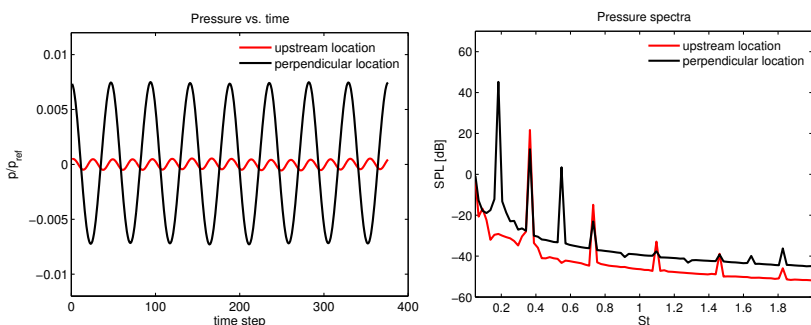


**Figure 4.10.** Time series and frequency spectra of pressure at an upstream and a perpendicular location. Evaluated on the fine grid at Mach=0.3.

Figure 4.11 illustrates the directivity at the shedding frequency. For comparison, a FW-H integral solution and the direct CFD simulation are included. The acoustic pressure magnitude is evaluated circumferentially at a radius of  $20 d$ . In the region trailing the cylinder, the pressure is omitted, since hydrodynamic pressures of the wake will dominate the acoustic pressure. The FW-H integral solution solves the same linear-propagation problem, with exactly the same sources as the WEM solution. These two solutions should therefore be closely related. The CFD solution on the other hand, is solved using the compressible flow equations with a finite volume method. No approximations are introduced in the CFD solution, regarding linear wave propagation in a uniform flow. Differences of the CFD solution and the analogy formulations therefore describe how the assumptions in the analogy influence the solution. However, the CFD solution will also be subjected to errors related to the solution procedure. It should be more prone to numerical errors in the acoustic propagation due to the properties of the discretization.

Comparing the three solutions, the analogy solutions are close to identical,

while the CFD solution starts to show slight differences with increased Mach number. The difference between the solutions can be related to dissipation errors in the CFD solution or assumptions made in the analogy. As the Mach number increases the resolution in terms of points per wavelength decreases in the CFD solution, which would suggest that dissipation could be an issue with the higher Mach number. However, the analogies also assume that the flow through which the acoustic waves propagate is homogeneous. As the wavelength is reduced and Mach number is increased, this assumption becomes more questionable.

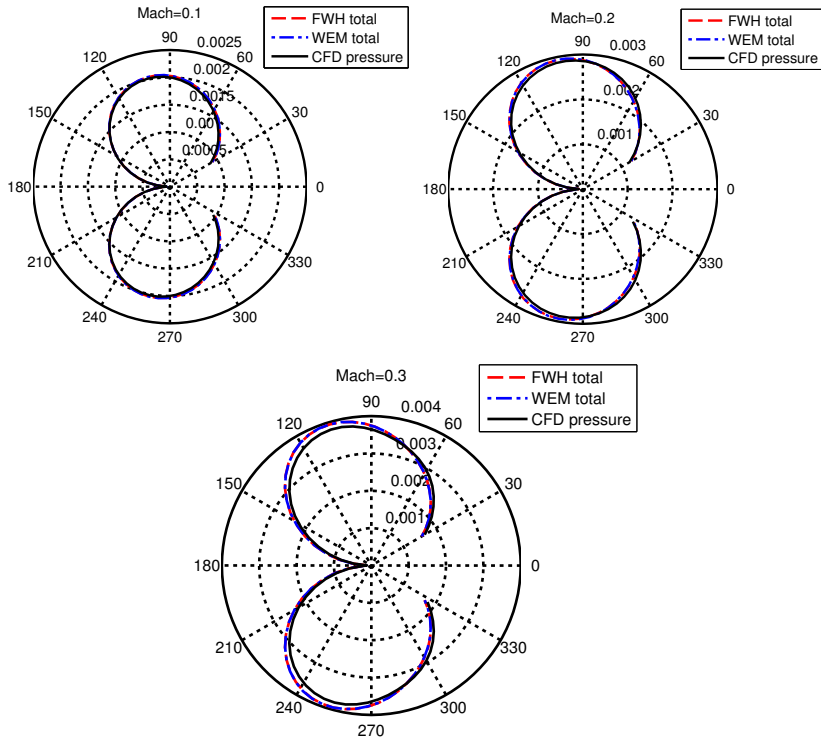


**Figure 4.11.** Directivity plot at a radius of  $20d$  for the shedding frequency.

A quantitative assessment of the pressure field at the shedding frequency is shown in Figure 4.12. Pressure normalized by the dynamic pressure is presented on a region covering  $50d \times 50d$ . At  $M_\infty=0.1$ , both methods show similar results. With higher Mach number, slight differences appear in the magnitude of the acoustic waves. However, the overall prediction is very similar for the two simulations.

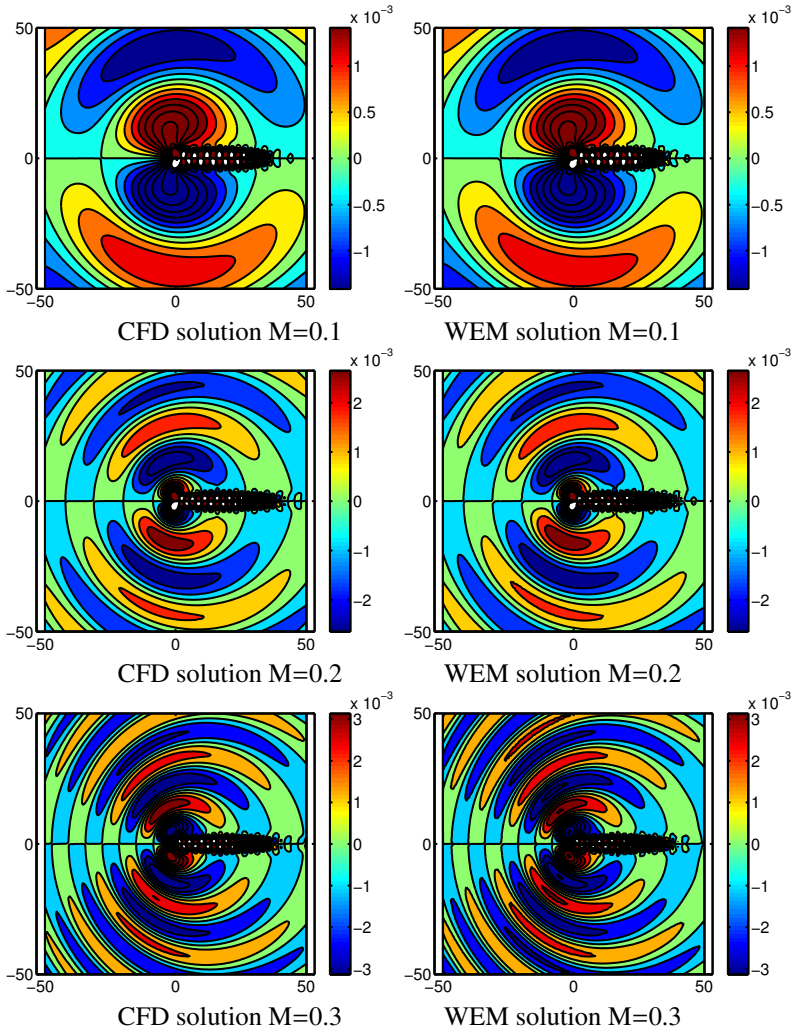


**Figure 4.12.** Acoustic pressure at the shedding frequency computed with CFD and WEM for three different Mach numbers.

## 4.5 Conclusions

In this chapter sources of different character have been introduced in the WEM. It is shown how a monopole source can be extended to dipole and quadrupole sources by adding a derivative to the Green's function. A mean flow can also be included by using a Prandtl-Glauert transformation. The point sources show ex-

cellent agreement with the analytical solution of the Green's function.

The simulation of the co-rotating vortex pair uses a source that is described by an analytical flow field. However, the solution is described on a discrete grid and then transferred to the acoustic simulation. The sources are described using two different aeroacoustic analogies, Lighthill and Vortex Sound Theory. The two analogies gave identical results for the computed cases and compare well with the analytical solution of the acoustic far-field.

In the cylinder case, a uniform mean flow is included in the wave operator and the sources are computed using CFD simulations. Since no analytical solution exists for this case, the results are compared to the pressure extracted directly from the CFD simulations. The results are in good agreement with each other. However, slight differences in amplitude and directivity start to appear as the Mach number is increased. This can either be a result of the CFD grid being too coarse to fully resolve the acoustic waves or it can also be related to the flow field used in the acoustic propagation. The flow field is assumed to be uniform in the propagation which might not be a good assumption as the Mach number increases.



# 5

## Fast matrix assembly technique

The WEM is an efficient procedure for solving linearized harmonic propagation equations in terms of points per wavelength. However, the procedure includes the computation of a Moore-Penrose pseudo-inverse which is performed at each point in the computational domain. When this is performed in a serial manner through a single value decomposition, it is very time consuming. It might even take more time than the inversion of the overall systems matrix. In the following chapter, which can be seen as an extended summary of Paper B, a method using a regular grid is presented. The structure of the regular grid is used to avoid the repeated evaluation of the pseudo-inverse. Furthermore, a method to introduce an irregular region in this regular grid is also described. This allows the method to be used without the limitation of a regular grid structure in all the domain.

### 5.1 Process for background matrix

As described in Chapter 3, the assembly of the system matrix includes the evaluation of a pseudo-inverse at each of the nodes in the domain. This procedure will relate each node to its neighbours and give the values to be introduced in the system matrix. By repeating this for each node, all the rows of the matrix can be entered. For an irregular grid, each row will have its own separate values depending on the local grid topology. The result of the pseudo-inverse is depending on the position of the neighbours with respect to the node at which the evaluation is performed. Therefore, an irregular grid will give different results at all nodes.

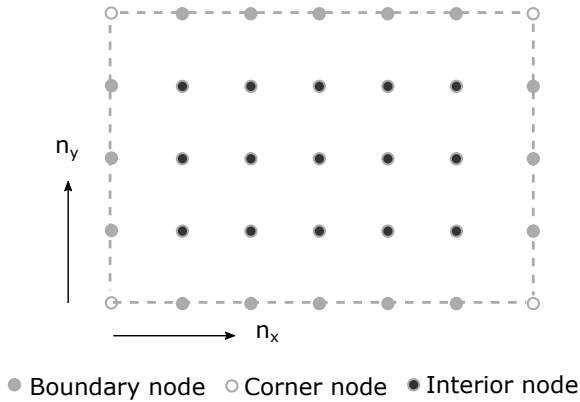


**Figure 5.1.** Different node types.

If the grid is regular, the relation to the neighbouring nodes will be the same at all positions. This provides a possibility to reuse the result at one node for all the nodes in the domain.

A regular grid can also be created using a certain structure, which gives knowledge of how the nodes are connected. By using this structure, the positions of the different values from the pseudo-inverse can be entered on each row. One row of the system matrix can therefore be used to describe the remaining rows.

There will be regions of the grid that cannot be created using this regularity. Even though the grid is fully equidistant, the outer boundaries will still differ from the internal nodes. This is due to the different number of neighbours and boundary conditions, resulting in different matrix entries for these nodes.

Regions where the pseudo-inverse will be different are illustrated in Figure 5.1. These regions, four boundary faces, four corners and internal nodes, will give a total of 9 different evaluations. If the domain is extended to three dimensions two more boundary regions and four more corners will be added giving a total of 15. This is a significant reduction from the evaluation at every node, which is otherwise needed.

### 5.1.1 Plane wave in a pipe

To investigate the possible speed-up using a method based on a regular grid, plane wave propagation is considered. This case is described in Figure 5.2 and will give plane waves propagating through a two-dimensional pipe. The first pipe end is defined by a Dirichlet boundary condition, setting the pressure to unity. The second is defined by an impedance boundary condition, which is set to let the

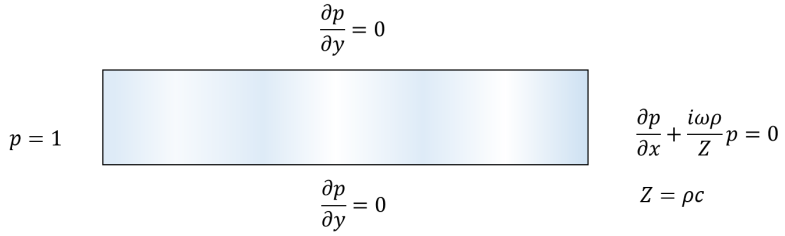


**Figure 5.2.** Plane wave setup.

waves propagate out of the pipe. At the walls, a Neumann boundary condition is used, imposing a zero gradient condition.

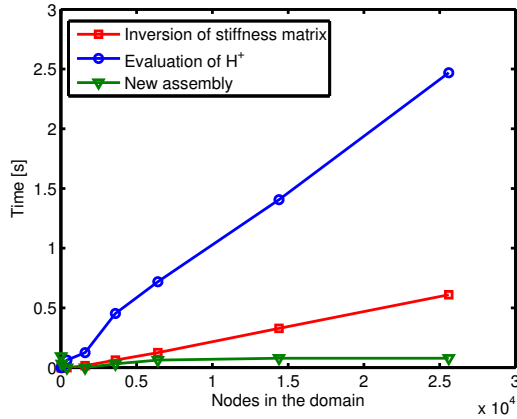


**Figure 5.3.** Time of fast assembly and pseudo-inverse evaluation at every node.

The new assembly process decreases the assembly time significantly. This is shown in figure 5.3, where the new assembly time is compared to the time it takes to perform the pseudo-inverse at each node. The time to invert the entire system matrix is also included in the figure. For this case the evaluation of the pseudo-inverse at every node takes longer time. The pseudo-inverse evaluations will also scale linearly with the number of nodes in the domain, which is not the case for the new assembly process. The new assembly will therefore give a considerable reduction in solution time.

The plane wave propagation can be described analytically through a 1D wave propagation. This solution can then be compared to the WEM solution, where the error defined by the deviation of the computed pressure to the analytical solution is

$$\epsilon = \frac{1}{N} \sum_{n=1}^N \frac{p_n - p_n^{ref}}{p_n^{ref}}. \quad (5.1)$$

$N$  is then the number of nodes in the evaluation,  $p_n$  is the computed pressure at node  $n$  and  $p_n^{ref}$  is the analytical solution at node  $n$ . Figure 5.2 shows the quite rapid decreasing error of the WEM solution which is compared to three FDM solutions<sup>35</sup> of the same problem. The WEM solution starts to give reasonable accuracy with as few as two to three points per wavelength. Which is very good considering the Nyquist criteria, stating that the absolute minimum needed is two points. The reason for the lower error in the WEM solution is mainly due to the low dispersion error of this method. This is an important advantage in many aeroacoustic analysis, especially when higher frequency and many wave lengths are considered. At only a few points per wavelength the WEM therefore outperforms all the FDM solutions. In terms of error reduction it will give a similar result as the 4th order FDM.

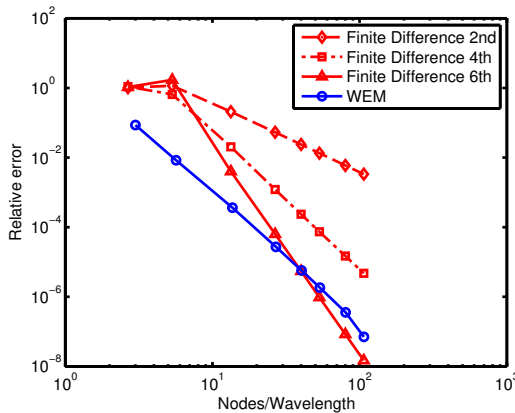


**Figure 5.4.** Error with increasing node density for the WEM and three different finite difference schemes.

## 5.2 Process with irregular region

The procedure described previously will be significantly limited by the regular grid that is needed. By considering the grid in different regions, this requirement can be dropped for parts of the domain. As an example, if a solid irregular object is introduced in the domain. The grid in the close proximity to the object will need to account for the object. However, most of the grid need not be affected by this. Thus a local re-meshing of this region can account for the irregularity. By doing so, a major part of the grid will still consist of the regular grid and can still take

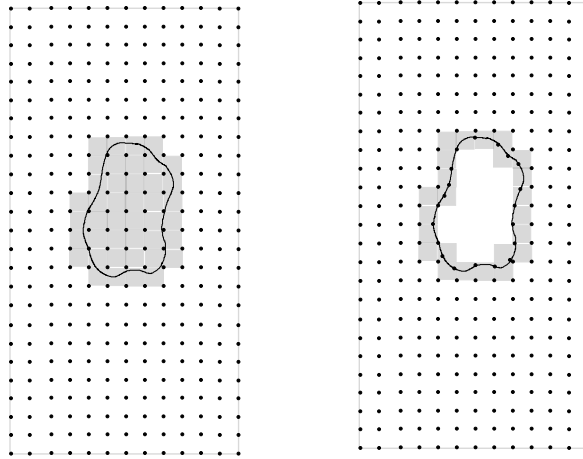


**Figure 5.5.** Regular grid with object.

advantage of the previously described method. The pseudo-inverse then only has to be re-evaluated for the nodes in the irregular region.

Irregularities can also consist of inhomogeneities in the flow, since this will effect the wavenumbers in the WEM discretization. For these cases the pseudo-inverse will need to be re-evaluated in the region with inhomogeneous flow. For the cylinder case considered in Chapter 4, this would typically correspond to the source region.

### 5.2.1 Local remeshing

The re-meshing process should be able to capture the geometrical features of the object such as boundary nodes and also exclude nodes that are inside the object. This type of procedure can be performed in a number of different ways. One would be to cut the region out of the grid and then introduce a new mesh, which is connected to the regular grid at the intersections. Another is to reposition the nodes to account for the object. In both these cases the pseudo-inverse then needs to be re-evaluated for the nodes in this new region and the corresponding rows and columns are re-assembled in the system matrix. The nodes connecting the two grids will also have to be re-evaluated since neighbours in the stencil will change.

To identify which nodes are influenced by the object, the elements which are inside and intersected by the object are identified. This is done by first finding all the nodes inside the object. The elements connected to these nodes are then marked, illustrated on the left side of Figure 5.5. By finding marked elements

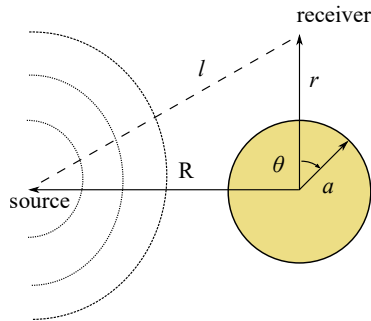


**Figure 5.6.** Schematic sketch of a monopole scattered by a cylinder.

that have nodes on both sides of the object, the elements which should contain boundary nodes are found. The elements marked by an irregular object are shown in the right part of Figure 5.5. The re-meshing is then performed by projecting the internal nodes within the marked elements onto the surface. These nodes will therefore be boundary nodes and the appropriate boundary conditions are then applied. After the nodes are projected, the elements within the object are deleted and the corresponding rows in the system matrix are nullified.

By performing these, steps the grid has been updated to account for the object by moving nodes to the surface of the object and deleting the elements inside the object.

To finalize the procedure, the rows in the system matrix for all the nodes that are in elements that are in connection to the boundary of the object needs to be evaluated. It is not enough to only consider the nodes on the surface. The pseudo-inverse will change for the nodes that have the boundary nodes in their stencil as well. Therefore, all of these nodes should be re-evaluated. After this procedure the system matrix is fully updated. This way of re-meshing by moving nodes also means that the system matrix will still have the same size, since no new nodes are introduced.

To test the method of including an irregular part of the domain, the acoustic scattering of a monopole source by a cylinder is considered. In Figure 5.6, the relevant variables for the setup are illustrated. In these computations the radius of the cylinder is specified to unity,  $a = 1$ , with receivers distributed circumferentially at a distance of  $r = 3a$ . The monopole source is of unit strength and is located at distance of  $R = 6a$ . The solutions are computed for three different wave numbers,  $ka = \pi$ ,  $ka = 2\pi$  and  $ka = 8\pi$ .

The results of the WEM computation is compared to an analytical solution which is described in Paper B in Part II or further in Khalighi<sup>16</sup>. Figure 5.7 shows the computed pressure amplitude of the circumferential receivers compared to this analytical solution. The WEM solution is in good agreement with the analytical solution.

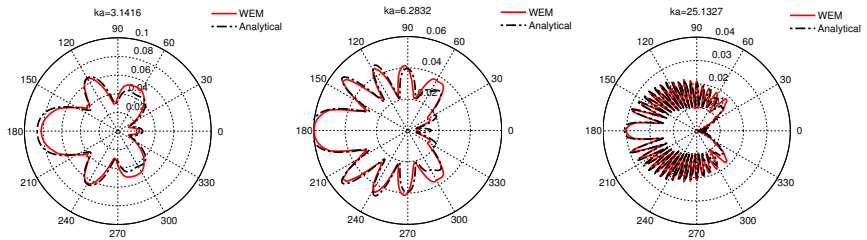


**Figure 5.7.** Pressure on receivers at a radius of  $3a$  for  $ka = \pi$ ,  $ka = 2\pi$  and  $ka = 8\pi$ .

### 5.3 Conclusions

In this section, a method to reuse the result of the pseudo-inverse at one location for a large part of the domain is presented. Since this is a time consuming part of the system matrix assembly a considerable speed-up is achieved in doing so. The plane wave propagation case used for the evaluation also highlights the efficiency of the WEM. Reasonable accuracy is achieved at just a few points per wavelength. It is also shown that the limitations of the regular grid can be circumvented by a local re-evaluation of the pseudo-inverse.



# 6

## Summary and Outlook

### 6.1 Conclusions

This work aimed at using the WEM in an aeroacoustic analogy framework. In this thesis two main parts have been investigated and developed. The first is directly related to aeroacoustic analogies, where aeroacoustic sources have been defined and then propagated using the WEM. The second part is related to the assembly process in the WEM, where a regular grid with irregular regions is used to minimize the assembly time. The following main conclusions may be drawn:

- The introduction of sources has been successfully implemented in the process, both for monopole and multipole sources. By using Prandtl-Glauert transformation the sources are also possible to use with the effect of a mean flow. Furthermore, distributed sources have also been successfully transferred to the acoustic grid from analytical and CFD solutions.
- By using a regular grid, a considerable speed-up is achieved compared to using a process where the pseudo-inverse is evaluated at each node. By allowing irregular regions, the process also becomes less restrictive as objects can be included in the domain.

### 6.2 Reflections and limitations

The method presented in the current work was evaluated in 2D. A 2D formulation is very convenient when the objective is to develop and verify simulation

procedures. However, the usefulness is also very limited, since most practical flow acoustic problems are in 3D. There are cases where both the flow and acoustic propagation can be described in 2D. In general, this is true for 2D flows at low Reynolds numbers. By extending the method to 3D, the range of application would be significantly increased.

The use of an aeroacoustic analogy also limits the range of application. In the formulations used, the flow and acoustic propagation are decoupled. The decoupling assumes that the flow source region is not influenced by the acoustic propagation. However, interactions between the flow and acoustic fields are permitted if they are included in the source computation and are properly resolved. A situation where the decoupling fails is therefore when backscattering from outside this region interacts with the flow. This might be the case when shedding is triggered by acoustic waves.

In the current work, the flow is solved in time domain, whereas the acoustic propagation is solved in frequency domain. This is efficient for each of the computations. However, it also means that the sources have to be transformed from time to frequency domain. To allow the transformation, a sufficient amount of time data needs to be stored. For large scale flow simulation this can be a limiting factor.

By using a uniform mean flow, convection is included in the acoustic propagation, extending the range of Mach numbers where it is applicable. The uniform flow will be closely related to the actual flow in the far field region. However, the near field and wake cannot be described properly by this assumption. The effect of the flow will typically increase with higher frequency and higher Mach number when these regions are not compact.

Regarding the fast assembly process, the regular grid gave a substantial speed-up of the assembly process. In this work, an irregular region in the form of a solid object was considered, which introduced wall boundaries in the computational domain. The grid was re-meshed for the irregular region close to the wall. However, the irregularity could also have consisted of inhomogeneous flow. Local regions of inhomogeneous flow could also have been added. The pseudo-inverse would then have to have been re-evaluated in these regions.

The re-meshing procedure described showed an approach to integrate an irregular region in the form of a solid object. This was achieved by repositioning the nodes to account for the object. While this was convenient, since no new nodes were introduced, and the system matrix was still the same size. It also limits the geometrical features that can be captured. If the geometrical features are smaller than the grid distance, more advanced meshing procedures can be used to include these.

### 6.3 Future work

To extend the area of application, the method should be evaluated with 3D problems. This will make it valid for more realistic cases. The flow and source region around vehicles and aircraft is 3D, due to the geometrical shape and high Reynolds number. The solver used in this work is valid for 3D, however the Green's functions used in the source introduction will need to be updated from 2D to 3D.

A natural continuation of this work will also include scattering of surfaces by the acoustic waves and a non-uniform mean flow. Thus, giving the method full advantage of being an volume discretizing method. This would enable the use for scattering of aeroacoustic sources from aircraft structures such as landing gear, wing trailing edges, struts or other external features.

A vast number of aeroacoustic analogies and decoupling procedures are available within aeroacoustics. Their uses are related to the assumptions made in the derivations. The Vortex Sound Theory by Howe naturally relates the acoustic propagation to a potential flow by using the total enthalpy as acoustic variable. The formulation might also give a less extended source region due to the vortex based formulation.

The assembly method should also be investigated further. There are many different aspects of this that could be continued. Especially the re-meshing procedure which can be developed further by applying a more robust way of re-meshing the irregular region.

The continuation of the work with the WEM for aeroacoustics is considered to extend the applicability to larger problems and provide an efficient propagation method which can include the effect of flow and scattering.



# Bibliography

- [1] European Aviation Group of Personalities, A Vision for 2020, Advise to European Commission, 2001.
- [2] High Level Group on Aviation Research, Flightpath 2050, Europe’s Vision for Aviation, EUR 098 EN, 2011.
- [3] S. K. Lele and J. W. Nichols, “A second golden age of aeroacoustics?,” *The Royal Society*, 2014.
- [4] T. Colonius and S. K. Lele, “Computational aeroacoustics: progress on nonlinear problems of sound generation,” *Progress in Aerospace Sciences*, vol. 40, p. 345–416, 2004.
- [5] C. K. W. Tam, “Computational aeroacoustics: Issues and methods.,” *AIAA Journal*, vol. 33, p. 1788–1796, 1995.
- [6] M. Lighthill, “On sound generated aerodynamically. I. General theory,” *Proceedings of the Royal Society of London*, vol. 211, pp. 564–587, 1952.
- [7] M. Lighthill, “On sound generated aerodynamically. II. Turbulence as a source of sound,” *Proceedings of the Royal Society of London*, vol. 222, pp. 1–32, 1954.
- [8] N. Curle, “The influence of solid boundaries upon aerodynamic sound.,” *Proceedings of the Royal Society of London*, vol. 231, pp. 505–514, 1955.
- [9] J. Ffowcs-Williams and D. Hawkings, “Sound generation by turbulence and surfaces in arbitrary motion.,” *Proceedings of the Royal Society of London*, vol. 264, pp. 321–342, 1969.
- [10] A. Powell, “Theory of vortex sound.,” *AIAA Journal*, vol. 36, pp. 177–195, 2002.
- [11] M. S. Howe. *Theory of Vortex Sound*. Cambridge University Press, Cambridge, UK, 2002.

## BIBLIOGRAPHY

- [12] P. Martínez-Lera, A. Mueller, C. Schram, P. Rambaud, W. Desmet, and J. Anthoine., “Robust aeroacoustic computations based on curle and powell analogies,” *ISMA Leuven Belgium*, 2008.
- [13] C. Wagner, T. Huttli, and P. Saugaut, *Large-Eddy Simulation for Acoustics*. Cambridge University Press, 2007.
- [14] A. Najafi-Yazdi, G. A. Bres, and L. Mongeau, “An acoustic analogy formulation for moving sources in uniformly moving media,” *Proceedings of the royal society*, vol. 467, pp. 144–165, 2011.
- [15] A. A. Oberai, F. Roknaldin, and T. J. R. Hughes, “Computation of trailingedge noise due to turbulent flow over an airfoil,” *Journal of Acoustical Society of America*, vol. 40, no. 11, pp. 2206–2216, 1964.
- [16] Y. Khalighi, *Computational aeroacoustics of complex flows at low Mach number*. PhD thesis, Stanford University, 2010.
- [17] C. K. W. Tam. *Computational aeroacoustics: a wave number approach*. Cambridge University Press, Cambridge, UK, 2012.
- [18] C. Bogey and C. Bailly, “A family of low dispersive and low dissipative explicit schemes for flow and noise computations,” *Journal of Computational Physics*, vol. 194, pp. 194–214, 2004.
- [19] G. Efraimsson, J. Gong, M. Svärd, and J. Nordström, “An investigation of the performance of a high-order accurate navier– stokes code,” *European Conference on Computational Fluid Dynamics ECCOMAS CFD, The Netherlands*, 2006.
- [20] J. E. Caruthers, J. C. French, and G. K. Raviprakash, “Green function discretization for numerical solution of the Helmholtz equation,” *Journal of Sound and Vibration*, vol. 187, no. 4, pp. 553–568, 1995.
- [21] J. E. Caruthers, R. C. Engels, and G. K. Raviprakash, “A wave expansion computational method for discrete frequency acoustics within inhomogeneous flows,” *AIAA/CEAS aeroacoustics conference, State College, Pennsylvania, USA*, 1996.
- [22] J. E. Caruthers, J. S. Steinhoff, and R. C. Engels, “An optimal finite difference representation for a class of linear PDE’s with application to the Helmholtz equation.,” *Journal of Computational Acoustics*, vol. 7, no. 4, pp. 245–252, 1999.
- [23] G. Ruiz and H. J. Rice, “An implementation of a wave-based finite difference scheme for a 3-d acoustic problem,” *J Sound Vib*, vol. 256, pp. 373–381, 2002.

- [24] L. B. Rolla and H. J. Rice, “A forward-advancing wave expansion method for numerical solution of large-scale sound propagation problems,” *Journal of Sound and Vibration*, vol. 296, pp. 406–415, 2006.
- [25] C. J. O’Reilly, G. Efraimsson, J. Hammar, and U. Emborg, “Numerical investigations of self-sustained shock oscillation acoustics,” *10th International Conference on Flow-Induced Vibration and Flow-Induced Noise, Dublin*, 2012.
- [26] C. J. O’Reilly, “A wave expansion method for acoustic propagation in lined flow ducts,” *Applied Acoustics*, vol. 90, pp. 54–63, 2015.
- [27] H. Liu, *Wave Modeling Techniques for Medium and High Frequency Vibroacoustic Analysis Including Porous Materials*. PhD thesis, Doctoral Thesis KTH Sweden, 2014.
- [28] M. S. Howe. *Acoustics of Fluid-Structure Interactions*. Cambridge University Press, Cambridge, UK, 1998.
- [29] A. Hirschberg and S. W. Rienstra. *An Introduction to Acoustics*, Eindhoven University of Technology, 2004.
- [30] X. Gloerfelt, C. Bailly, and D. Juve, “Direct computation of the noise radiated by a subsonic cavity,” *Journal of Sound and Vibration*, vol. 266, pp. 119–146, 2003.
- [31] P. Saffman, “Vortex dynamics,” *Cambridge University Press*, pp. 253–254, 1993.
- [32] L. Qu, C. Norberg, L. Davidson, S. Peng, and F. Wang, “Quantitative numerical analysis of flow past a circular cylinder at reynolds number between 50 and 200,” *Journal of Fluids and Structures*, vol. 39, pp. 347–370, 2013.
- [33] J. Park, K. Kwon, and H. Choi, “Numerical solutions of flow past a circular cylinder at reynolds numbers up to 160,” *KSME International Journal*, vol. 12, pp. 1200–1205, 1998.
- [34] C. H. Williamson, “Oblique and parallel modes of vortex shedding in the wake of a circular cylinder at low reynolds numbers,” *Journal of Fluid Mechanics*, vol. 206, pp. 579–627, 1989.
- [35] B. Gustafsson, *High order difference methods for time dependent PDE*. Springer Series in Computational Mathematics, 2008.



**Part II**

**APPENDED PAPERS**

